Journal Pre-proof

Oleic Acid Fuels Cisplatin-Resistant Ovarian Cancer Through FABP4-Driven Lipid Uptake

Ana Maria Isac, Andres Valdivia, Didi Zha, Yinu Wang, Vanessa Hernandez, Guangyuan Zhao, Chinmayee Vallabh Prabhu Dessai, Ujin Kim, Annapurna Sai Josyula, Wenan Qiang, Sandra Orsulic, Ji-Xin Cheng, Daniela Matei

PII: S2212-8778(26)00058-X

DOI: https://doi.org/10.1016/j.molmet.2026.102374

Reference: MOLMET 102374

To appear in: *Molecular Metabolism*

Received Date: 16 December 2025

Revised Date: 8 April 2026

Accepted Date: 15 April 2026

Please cite this article as: Isac AM, Valdivia A, Zha D, Wang Y, Hernandez V, Zhao G, Dessai CVP, Kim U, Josyula AS, Qiang W, Orsulic S, Cheng J-X, Matei D, Oleic Acid Fuels Cisplatin-Resistant Ovarian Cancer Through FABP4-Driven Lipid Uptake, *Molecular Metabolism*, https://doi.org/10.1016/j.molmet.2026.102374.

Oleic Acid Fuels Cisplatin-Resistant Ovarian Cancer Through FABP4-Driven Lipid Uptake

Ana Maria Isac[1], Andres Valdivia[1], Didi Zha[1], Yinu Wang[1], Vanessa Hernandez[1], Guangyuan Zhao[1], Chinmayee Vallabh Prabhu Dessai[2], Ujin Kim[1], Annapurna Sai Josyula[1], Wenan Qiang[1], Sandra Orsulic[3,4], Ji-Xin Cheng[2], Daniela Matei[1,5,6]

[1]Department of Obstetrics and Gynecology, Feinberg School of Medicine, Northwestern University, Chicago, IL 60611, USA

[2]Department of Biomedical Engineering, Boston University, Boston, MA, 02155, USA

[3]David Geffen School of Medicine, University of California, Los Angeles (UCLA)

[4]VA Greater Los Angeles Healthcare System, Los Angeles, CA, USA

[5]Robert H. Lurie Comprehensive Cancer Center, Feinberg School of Medicine, Northwestern University, Chicago, IL 60611, USA

[6]Jesse Brown VA Medical Center, Chicago, IL, 60612, USA

Correspondence:

Daniela Matei, 303 E Superior St, Lurie 4-220, Chicago, IL 60611, USA
daniela.matei@northwestern.edu

Conflict of interest: The authors declare no conflict of interest related to this material.

Abstract

Background: Ovarian cancer (OC) depends on lipids as fuel for metastasis and growth. We previously showed that cisplatin resistant (Pt-R) OC cells uptake higher amounts of fatty acids (FAs) compared to sensitive (Pt-S) cells, a process which facilitates cancer cell survival under cisplatin-induced oxidative stress.

Methods: Isogenic pairs of Pt-S and Pt-R OC cell lines were cultured in low serum conditions supplemented with either 50 µM oleic acid (OA, unsaturated) or 50 µM palmitic acid (PA, saturated) and used for viability assays, RNA-Sequencing, and cell cycle analysis. The effects of an OA enriched diet were assessed in intraperitoneal ovarian xenografts. The FABP inhibitor BMS-309403 was used to block lipid import *in vitro* and *in vivo*.

Results: Pt-R cells were less viable than Pt-S cells under serum depletion and OA rescued starvation induced inhibition of cell proliferation, with more significant effects in Pt-R compared to Pt-S cells. RNA-sequencing showed that OA promoted upregulation of cell cycle-related pathways, including *G2/M checkpoints*, driven by the transcription factor *E2F1*. Supplementation with OA increased S- and G2/M phase cell populations in both Pt-S and Pt-R cells ($p<0.05$) and *E2F1* inhibition reduced OA-induced cell proliferation. An OA enriched diet promoted the growth and peritoneal dissemination of Pt-R ovarian xenografts. When co-cultured with adipocytes, Pt-R cells expressed higher levels of FA transporter proteins FABP4 and CD36 compared to sensitive cells and FABP4 expression was upregulated in paired metastatic and recurrent vs. primary human ovarian tumors ($p<0.05$). An FABP inhibitor sensitized OC cells to cisplatin and suppressed the *in vivo* growth of Pt-R xenografts and patient derived xenografts.

Conclusions: Pt-R OC cells harbor heightened dependence on unsaturated FAs compared to Pt-S cells and upregulate key transporters to increase FAs uptake. OA supports the proliferation of Pt-R

cells *in vitro* and *in vivo* and a combination of carboplatin and FABP4 inhibitor reduces OC growth *in vivo.* These findings suggest that lipid composition may influence therapeutic response and raise important considerations for dietary guidance in patients with cancer.

Introduction

Ovarian cancer (OC) remains one of the leading causes of cancer-related deaths in women, primarily due to late-stage diagnosis and limited treatment options [1]. Understanding the molecular mechanisms that drive OC progression and resistance to treatment is crucial for identifying potential therapeutic targets [2]. Recent evidence suggests that metabolic reprogramming, including alterations in lipid metabolism, plays a key role in OC progression and platinum resistance [2, 3]. We previously reported that Pt-R OC cells uptake increased amounts of FAs which were used for β-oxidation [3]. Among the various lipid species, mono-unsaturated fatty acids (MUFAs), particularly oleic acid (OA), have gained attention for their potential to modulate cancer cell behavior and influence tumor progression, with effects varying based on the cancer type [4-7].

Oleic acid (C18:1), a predominant MUFA found in various dietary sources such as olive oil [8], is the main MUFA in the human diet [9] and the principal product formed by stearyl-CoA desaturase 1 (SCD1) from stearic acid (C18:0) [10]. OA is a key component of cellular membrane phospholipids [11], and has been implicated in a range of cellular processes. For instance, OA was found to regulate gene expression and signaling pathways, such as core metabolic pathways that promote the differentiation of non-activated T cells into IL-9 producing cells [12]. OA has also been reported to downregulate the expression of cholesterol transport-related genes [13] and to reduce low-density lipoproteins (LDL) [14]. OA can also regulate the synthesis and activity of antioxidant enzymes [15]. These properties render OA highly beneficial, contributing to a range of positive physiological effects, however, in cancer, its activities can be divergent [16]. In the context of OC, the balance between unsaturated fatty acids (UFAs) and saturated fatty acids (SFAs) – which is mediated by SCD1, plays a key role in mediating tumor cell fate under metabolic stress, where depletion of UFAs leads to increased endoplasmic reticulum (ER) stress and initiates tumor cell death [17]. SCD inhibitors blocked prostate and breast cancer cell proliferation in low serum conditions [18, 19] and these effects

were rescued by exogenous supply of OA. Similarly, depletion of OA inhibited the proliferation of acute myelogenous leukemia and lymphoma cells [20]. These data support the significance of UFAs which are either newly synthesized or imported from the extracellular milieu to maintaining the energetic or structural needs of cancer cells. Despite these reports that have linked lipid metabolism to cancer progression, the mechanisms through which specific FAs, like OA, might influence tumor biology and resistance to treatment remain not fully understood. This study aimed to determine how OA promotes the growth of chemo-resistant OC cells and tumors.

Cancer cells can either synthesize lipids through de novo lipogenesis or uptake lipids from the tumor milieu. Lipid import is mediated by transporters and has gained increasing attention as a potential pharmacologic target. Fatty acid binding proteins (FABP), such as FABP4 and FABP5, reversibly bind hydrophobic ligands, like long-chain fatty acids, to facilitate uptake and distribution in cells [21], where they can be utilized for energy production, membrane biosynthesis, and as signaling intermediates [22]. FABP4 was reported to drive metastasis [23] and mediate resistance to platinum [24] in OC models. However, it remains unknown which FAs are preferentially taken up by cancer cells and the mechanism by which they fuel cancer growth. Here we investigated whether and how OA is imported by cancer cells to support tumor growth and the metabolic rewiring of cancer cells linked to the acquisition of chemotherapy resistance.

Materials and Methods

Sex as a biological variable.

Ovarian cancer is relevant in females, therefore only females were included in animal experiments and all patient samples were collected from women.

Cell lines and reagents.

OVCAR5 cells were obtained from Dr Marcus Peter, Northwestern University. OVCAR5 platinum resistant (Pt-R) cells were generated in our laboratory by administering consecutive cisplatin treatments according to a previously described protocol [25]. PE01 and PE04 cells were purchased from Sigma-Aldrich (#10032308-1VL, #10032309-1VL). Visceral preadipocytes (VNPAD) were provided by Dr. Aloysius Klingelhutz from University of Iowa [26, 27] and were differentiated into mature adipocytes according to a previously described protocol [28]. All cells were incubated at 37^{o}C, 5% CO_2 and used at low passage number (<10). The cell culture media are provided in Supplementary Table S1. The cell lines were authenticated by IDEXX BioAnalytics with STR profiling and regularly tested for mycoplasma contamination using the ATCC Universal Mycoplasma Detection Kit and the Charles River Animal Diagnostic Services. Bovine serum albumin (BSA) conjugated oleic acid (# O3008), palmitic acid (# P0500), the E2F1 inhibitor HLM006474 (#SML1260-5MG), DMSO (# D2650), and Tween 80 (#P4780) were purchased from Millipore Sigma. The FABP inhibitor BMS-309403 (HY-101903) and PEG300 (# HY-Y0873) were purchased from MedChemExpress. The chemically defined lipid concentrate (#11905031) was purchased from ThermoFisher and includes a mixture of saturated and unsaturated fatty acids and cholesterol. All primers, antibodies, and their suppliers are included in Supplementary Table S2 and S3, respectively.

Human specimens

Deidentified specimens of high-grade serous ovarian tumors and OC associated malignant ascites were collected from consenting donors under Northwestern University's approved protocol IRB#: STU00202468. Tumor tissues were minced and then enzymatically and mechanically dissociated into single cell suspension, as previously described [29]. Cells from ascites were pelleted by centrifugation, the red blood cells were lysed (cat. no. # R7757-100ML, Sigma) before use or cryopreserved until analysis. The deidentified clinical annotations for the primary OC cells are included in Supplementary

Table S4. A tissue microarray (TMA) containing matched primary, metastatic, and recurrent tumors from 21 patients with HGSOC was constructed and provided by Dr. Sandra Orsulic, University of California, Los Angeles (UCLA). Tumors are deidentified, clinically annotated and arrayed in triplicate on the TMA. The clinical data are included in Supplementary Table S5.

Adipocyte differentiation and co-culture with ovarian cancer cells

VNPAD pre-adipocytes were differentiated into mature adipocytes as previously described [28] . Briefly, the cells were cultured in pre-adipocyte growth medium (Cell applications, #811-500) until they reached confluency. The growth medium was then changed to Adipocytes Differentiation Media (Cell Applications #811D-250). The maturation of adipocytes was assessed by examining lipid droplets formation by using brightfield microscopy. Mature adipocytes were used for collection of conditioned media, and for co-culture experiments [30] with cancer cells fluorescently labelled with GFP (OVCAR5 Pt-S), or with TomatoRed (OVCAR5 Pt-R). For the co-culture, $2X10^6$ labeled OC cells were seeded in culture dishes containing a monolayer of mature adipocytes. The cells were grown together for 3 days before being separated by flow cytometry sorting (FACSMelody, BD Bioscience) using the fluorescent channels. The sorted OC cells after co-culture were used for subsequent experiments.

Cell proliferation assay

Cells were seeded in 96-well plates at a density of 500 cells per well. The CCK8 kit (APExBIO #K1018) was used to estimate cell viability as per manufacturer's instructions. The absorbance was measured at 450 nM by using the BioTek ELX800 microplate-reader. Results were then normalized to the confluence of the first day.

Immunohistochemistry (IHC)

IHC was performed using paraffin embedded xenograft tumors or HGSOC tumors included on a TMA. Ki-67 staining used an antibody from Abcam (cat# ab15580) at 1:200 concentration. Briefly, tissue sections were deparaffinized by incubating slides at 56^0 C for 30 minutes, followed by two 30-minute washes in xylene. Residual xylene was then removed by two 3-minute washes in 100% ethanol (EtOH), followed by 3-minute washes in 90% EtOH, 70% EtOH, 50% EtOH, and finally in dH_2O. The antigen retrieval was performed by incubating the tissue sections in citrate buffer (0.01 M citric acid monohydrate, 0.05% Tween-20, pH 6) for 30 minutes at 95^{o}C, and then left to cool at RT for 1 hour. The slides were then washed in PBS twice for 5 minutes, treated with 3% H_2O_2 for 15 minutes, and then washed with PBS three times for 5 minutes. The tissue sections were then blocked for 30 minutes at RT in 3% Non-Specific Goat Serum in PBS, before incubating them with primary antibody, overnight, at 4^{o}C. For immunohistochemical staining, the tissues were incubated with the DAKO LSAB2 System (Cat. No. #K0675, Agilent Technologies) biotinylated link for 15 minutes, washed with PBS three times for 5 minutes, and then incubated with the Streptavidin-HRP solution for 15 minutes, followed by three 5 minutes with PBS. The tissues were stained in the dark with the DAB solution (Cat. No. #K3467, Agilent Technologies) and the reaction was stopped by putting the slides in dH_2O. The slides were then counter stained with hematoxylin (Cat. No. #6765007, ThermoFisher) and mounted using the Dako Faramount Aqueous Mounting Media (Cat. No. #S302580-2, Agilent Technologies). Quantification of staining intensity was performed by using the DAB deconvolution method using ImageJ software. FABP4 staining used an antibody from Themofisher (cat. no. 12802-1-AP) at 1:200 concentration in the Northwestern University Pathology Core Facility following a similar protocol. FABP4 staining in cancer cells was scored in a blinded manner for intensity (0-3+) and percentage of cancer cells staining. An H score was calculated as the product between intensity and percentage of cancer cells staining. The H score was averaged across replicate tumors for each

condition and each patient (n=3 replicate per condition and per patient). Image color balance in every pixel was adjusted using ImageJ.

Half maximal inhibitory concentration (IC_{50}) determination

Dose response experiments were performed to measure the inhibitory effects of different compounds and to calculate IC_{50} values. Cells were seeded in 96-well plates at a density of 2000 cells per well and treated with a dose range of BMS and cisplatin for 72 hours (h). Cell viability at 72h was determined by using a CCK8 kit as described above or by live-cell imaging using the Incucyte system as previously described[17]. IC_{50} values were calculated in GraphPad Prism using a logarithm-normalized sigmoidal dose curve fitting.

RNA extraction and RT-qPCR

RNA was isolated using TRIzol (Invitrogen #T9424) according to the manufacturer's instructions. RNA concentrations were assessed using the Eppendorf BioSpectrometer® basic. The iSCRIPT cDNA synthesis kit (BioRad) was used to reverse transcribe 1 µg of total RNA into cDNA. The expression of the desired target genes was determined by Real-Time PCR amplification, using the iTAQ Universal SYBR green Supermix (Bio-Rad). Primers are listed in Supplementary Table S2. The following conditions were used on the AB 7900HT instrument (Applied Biosystems): 94ºC for 10 minutes, 40 cycles of amplification at 94ºC for 15 seconds, and 60ºC for 1 minute, followed by an extension step of 7 minutes at 72ºC. The relative mRNA levels were calculated by using the ΔΔCT method using GAPDH as the internal control. Results were plotted in graphs as means ± SD of three biological replicates per experimental group.

Cell cycle analysis using flow cytometry

Cells were seeded at a density of 300,000 cells per 6 cm dish and treated according to the experimental conditions. After trypsinization, cells were fixed using cold 70% ethanol and stored at 4^{o}C for a minimum of 15 minutes. The cells were stained with the BD Pharmingen™ PI/RNase Staining Buffer (# 550825) according to manufacturer's instructions and then analyzed by using the BD LSRFortessa™ Analyzer. The cell cycle distribution was analyzed using the FlowJo software, version 10.8.1 (BD Biosciences).

RNA-Sequencing library preparation and data analysis (pathway analysis)

For the RNA-Seq analysis of OC cells, total RNA was isolated using the RNeasy Mini Kit (QIAGEN, #74104). For xenografts, RNA was extracted using TRI reagent followed by the removal of genomic DNA using the RNeasy MinElute Cleanup Kit (QIAGEN, cat#: 74204). To ensure the purity and integrity of the RNA, the samples were treated with DNase I, and the 260/280 ratios had a minimum value of 1.8. The mRNA was isolated from 1 µg of total RNA using the NEBNext Poly(A) mRNA Magnetic Isolation Module (NEB #E7490). The RNA-Seq libraries were prepared using the NEBNext Ultra II RNA Library Prep Kit for Illumina (New England Biolabs, Inc. cat#: E7770S), sequenced, and analyzed to identify differentially expressed genes, as previously described [31]. The raw RNA-seq reads were aligned to the human reference genome GRCh38 ENSEMBL using HISAT2 and SAMtools. Mapped reads were then counted using the SubRead featureCounts program, the raw counts were normalized, and differential analysis of gene expression was conducted using the edgeR package in R. FDR was corrected for multiple hypothesis testing using Benjamini-Hochberg (BH) method. The data are deposited in GEO (GSE295220, token yrafksyadzadtod) and pathway and regulator analysis were performed using Metascape [32] and EnrichR [33]. Gene set enrichment analysis was conducted using Hallmark gene sets from Human Molecular Signatures Database (MSigDB).

Reverse Phase Protein Array (RPPA): Cells were cultured and treated as follows: control group (10% FBS), starvation (1% FBS for 72 hrs), OA (1% FBS for 24 hrs followed by supplementation with 50 μM OA for 48 hrs). Snap frozen cell pellets were processed for protein extraction and RPPA analysis at to the MD Anderson Cancer Center Proteomics Core Facility. Briefly, the samples were spotted on nitrocellulose –coated slides and probed with specific primary antibodies (n = 497 antibodies). Target proteins were detected by using a tyramide signal amplification system followed by DAB colorimetric development (GenPoint kit, Agilent). Slides were scanned using a Huron TissueScope to generate 16-bit TIFF images and spot intensities were quantified using Array-Pro Analyzer software. Relative protein levels were calculated by using RPPA Super Position and Concentration Evaluation (SPACE) by fitting dilution curves and determining the EC50 for each sample and interpolating in RPPASPACE (https://bioinformatics.mdanderson.org/public-software/rppaspace/).

Western blotting

Proteins were extracted by using RIPA buffer and the concentrations were quantified using the Bradford method (BioRad, #5000006). Proteins were resolved by SDS-PAGE and then transferred onto a PVDF membrane by using a wet electrophoresis system. Membranes were blocked in 5% BSA TBS–Tween for a minimum of one hour and then incubated overnight at 4^{o}C with primary antibodies (Supplementary Table S3., 1:1000 dilution). Incubation with secondary antibody (anti-rabbit/mouse-HRP, 1:1000 dilution) was performed at room temperature, for 1 h. Detection of chemiluminescence signal was performed using the SuperSignal West Pico PLUS (Thermo Fisher Scientific, cat #34580) and the ImageQuant LAS 4000 imaging system. For detection of additional proteins on the same membrane, the membrane was stripped using the Restore Western Blot Stripping Buffer (Thermo

Fisher Scientific, #21059), washed with TBS-Tween, blocked, and then re-incubated with another primary antibody.

In vivo experiments

Animal studies were approved by the Institutional Animal Care and Use Committee (IACUC) of Northwestern University (protocol IS00017063). Female 6-7 week old, athymic nude mice (*Foxnl*^{nu}) were purchased from Envigo. In one experiment, mice were randomly assigned to olive oil enriched diet (TD #240783, Inotiv, Lafayette, IN) vs isocaloric diet (TD#94045). After one week, mice were injected intraperitoneally (IP) with 2X10^6 OVCAR5 Pt-R cells. Mice were observed for 4 weeks while continuing the respective diets. At necropsy, tumor numbers, weights and volumes and ascites volumes were recorded. In a second experiment, mice were injected IP with 2X10^6 OVCAR5 Pt-R cells and then randomly assigned to IP treatment with carboplatin (20 mg/kg body weight) once a week, the FABP inhibitor BMS-309403 (15 mg/kg body weight) for five days a week, the diluent (10% DMSO, 40% PEG300, 5% Tween-80, 45% saline), or with carboplatin (20 mg/kg) and FABP inhibitor (15 mg/kg). Treatment was continued for 4 weeks. At necropsy, tumor numbers, weights and volumes and ascites volumes were recorded. Tumor volumes were calculated by measuring the tumor length (L), width (W), and height (H) using digital calipers and by utilizing the formula V = ½ x L x W x H. Tumors > 3mm in greatest diameter were aggregated and measured to calculate a total tumor volume per mouse. Lastly, a PDX experiment was performed under Northwestern University IACUC (protocol #IS00007992). Pieces of an ovarian tumor established from a consenting donor and obtained as previously described [29] were implanted SQ in female NOD SCID gamma (NSG) carrier mice (Jackson Laboratory) and allowed to grow up to 1cm diameter over approximately 3 months. The harvested PDX was examined by H&E staining and confirmed to maintain high grade serous histology by a board-certified pathologist. The harvested tumor was divided into equally sized fragments (~2 ×

2 × 2 mm) and re-implanted SQ in the dorsal region of female NSG mice. Once tumors in experimental mice reached 150 mm^3, mice were randomized to treatment with either diluent or BMS-309403 given IP (15 mg/kg body weight; 5 days per week, 5 weeks, n=7 mice/group). Treatment continued until at least one of the control mice developed tumor of 1500 mm^3 or toxicity was noted in any of the mice. Body weights were monitored weekly, and tumor sizes were measured by calipers twice-a-week. Tumor volumes were calculated as described above. Tumors were collected and processed as described above.

High Content Stimulated Raman Scattering (SRS) imaging and analysis

Tissue blocks embedded in OCT (Optimal Cutting Temperature) and stored at -80C were sliced at 10μm thickness using a Leica CM1950 cryostat and slices were placed on glass slides. After washing in 1X PBS solution, slices were sealed under a glass cover. To acquire hyperspectral SRS imaging data, the previously described mature homemade hyperspectral SRS (hSRS) system was used [17, 34]. The setup was built with a dual output laser (Insight DeepSee, Spectra Physics) with the laser source operating at 80 MHz. The recently developed method of high content SRS (h2SRS) imaging was employed [34, 35], involving acquisition of hSRS images and application of pixel-wise least absolute shrinkage and selection operator (LASSO) for spectral unmixing of images into biochemical maps. H2SRS of small field-of-view (FOV) images of the tissue were acquired and ImageJ grid stitching toolbox was utilized to stitch them into large-FOV image data. Denoising of large-FOV images used the spectral total variation algorithm [35, 36] and LASSO unmixed images into biochemical maps. Reference spectra for collagen were obtained by extracting the collagen signal from the tissue regions [37], while glycerol trioleate (Sigma Aldrich, #92860), and pure cholesterol (Sigma Aldrich, #C3045) samples were used as lipid and cholesterol standards, respectively. The cellular protein spectrum was extracted by using the cell spectrum from the cellular areas in the tissue and subtracting the lipids

spectrum. Lipids and proteins maps quantified the lipids in the cellular regions by manually annotating cells in the tissue images in ImageJ. The lipid signal was normalized to the cell protein signal in these regions. Statistical analysis used the t-test in the Origin Lab Software (n=7-8 tissue slides per group).

Statistical Analysis

Data were obtained from a minimum of three independent replicates. Statistical analysis was performed by using the GraphPad Prism 7 software. Comparison of multiple groups was performed using the two-way ANOVA statistical test, whilst comparison of two groups used unpaired t-tests. P-value <0.05 was considered statistically significant. Tumor volume growth data PDX experiment were analyzed by using linear mixed effects model to compare tumor growth patterns between groups (BMS-309403 vs control) over time. Tumor volumes was log2-transformed to satisfy the normality assumption, and predictors included time, treatment group and their interaction as fixed effects, and mouse as the random effect. Within-mouse correlation between longitudinal measurements was accounted for using autoregressive variance structure. Estimated marginal means were compared at various time points based on the model.

Results

Platinum resistant cells rely more on oleic acid compared to sensitive cells

Highly proliferating cancer cells undergo stress in the tumor microenvironment (TME) due to changes in pH or O_2 and absence of required nutrients [38]. OC cells are highly dependent on lipids for proliferation, migration and cell signaling [39]. To assess how exogenous lipids affect proliferation of OC cells we used sensitive (Pt-S) and cisplatin resistant (Pt-R) cells cultured under low serum conditions to simulate a stressful environment. Cells were supplemented with 50 μM oleic acid conjugated with BSA (OA, unsaturated) or palmitic acid (PA, saturated) and cell viability was monitored over 7 days (**Figs. 1A and B**). Two isogenic models were used, Pt-S and Pt-R OVCAR5

cells, previously described [29] and isogenic PEO1 (sensitive) and PEO4 (resistant) derived from tumors from the same patient at different stages during the disease course [40]. Cell morphology of Pt-S and Pt-R cells under full culture media, 1% serum and rescue with OA is shown in Supplementary **Figs. S1A-B**. Both cell types were sensitive to serum depletion, but Pt-R cells were less viable under serum depletion compared to Pt-S OC cells (Supplementary **Figs. S1C-D**). Notably, OA supplementation significantly promoted the proliferation of both sensitive and resistant cells. OA rescued Pt-R cells to a greater extent than Pt-S cells (268.4% vs 91.6% in OVCAR-5 and 38.1% vs 12.1% in PEO4 and PEO1, respectively; **Fig. 1C**, $p<0.01$). Combined, these results suggest that Pt-R cells were more dependent on unsaturated FAs for survival compared to Pt-S cells. In contrast, addition of a saturated FA (PA) did not rescue cell viability in either Pt-S or Pt-R OC cells (**Figs. 1A and B**). To investigate whether OA alone is responsible for the observed pro-proliferative phenotype, we assessed the effects of other lipids upon OC cell proliferation. The tested lipids included a chemically defined lipid concentrate which includes both unsaturated and saturated FAs, as well as cholesterol (Supplementary **Fig. S1E**), and conditioned media from adipocytes (Supplementary **Fig. S1F**). Lower concentrations of the lipid mix induced modest rescue of cell proliferation in both Pt-S and Pt-R cells, but higher concentrations were toxic to the cells (Supplementary **Fig. S1E**). Rescue effects induced by conditioned media from adipocytes were modest and not consistent (Supplementary **Fig. S1F**).

To demonstrate that these findings are relevant to human tumors, we tested the effects of OA in primary cells derived from HGSOC tumors or from OC-associated ascites. Tumor characteristics are included in Supplementary **Table S4**. Cell proliferation monitored by Incucyte demonstrates inhibition of cell proliferation under 1% serum for all primary cells analyzed and significant rescue by addition of OA (**Fig. 1D**). One of the primary cultures (PT168) derived from malignant HGSOC ascites was particularly sensitive to OA supplementation (**Fig. 1D)**. Together, these results show the effects of

unsaturated FAs, particularly of OA, in supporting the viability of OC cells under conditions of metabolic stress.

OA supports proliferation of OVCAR5 cells *in vitro* and *in vivo* by promoting cell cycle progression

To further characterize the effects of OA, we performed RNA-Sequencing analysis to identify the transcriptomic changes induced by 24 h treatment with OA in OVCAR5 cells. In Pt-S OVCAR5 cells there were 973 differentially expressed protein-coding genes (DEGs) between control (1% FBS) and OA-treated cells, with 300 upregulated and 673 downregulated transcripts (FDR<0.05; **Fig. S2A**). The top 25 upregulated genes in response to OA in Pt-S OC cells are included in Supplementary **Table S6**. In Pt-R OVCAR5 cells, 1364 genes were differentially expressed between control (1% FBS) and OA treated cells, 240 being upregulated and 1124 being downregulated (FDR<0.05; **Fig. 2A**). The top 25 upregulated genes after treatment with OA in Pt-R OC cells are included in Supplementary **Table S7**. Among the top upregulated genes in Pt-S cells, the mini-chromosome maintenance (*MCM*) transcripts *MCM2, -4, -6,* as well as the *MYBL2* gene – involved in cell proliferation and differentiation [41], *E2F2* and *-8* which regulate cell cycle progression [42], *FOSL-1* with roles in epithelial to mesenchymal transition (EMT), and *CXCL5* – an inflammatory chemokine that may play a role in cancer proliferation, migration, and invasion [43] were identified **(Fig. 2B)**. The *MCM* genes (*MCM3, -6, -10*) were among the top upregulated genes in Pt-R cells, as well as *SKP2* – a component of E3-ligase SCF complex, found to modulate the proliferation and tumorigenesis of glioma [44], and *CDKN3* – reported to promote OC cell proliferation and invasion [45] **(Fig. 2C)**. Pathway analysis of the upregulated genes revealed cell cycle related pathways such as: *cell cycle mitotic*, *cell cycle checkpoints*, *G2/M checkpoints* among the top 10 most significantly upregulated pathways in both cell

types **(Figs. 2D-E)**. The transcription factor E2F1 was identified as one of the main effectors in both Pt-S and Pt-R OVCAR 5 cells **(Figs. 2F-G)**.

Further, RPPA analysis of cells treated with OA vs 1% FBS identified 84 proteins differentially expressed after treatment with OA (FDR < 0.05). Pathway analysis of differentially expressed proteins identified "*G2/M transition of mitotic cell cycle", "Cell cycle G2/M phase transition" and "Positive regulation of cell proliferation"* among the top enriched pathways in OA-treated cells (**Fig 3A**, black arrows). Cell cycle analysis using PI staining and flow cytometry-based analysis confirmed that OA induced increased percentages of cells in S- and G2/M phases – from 6.95% to 11.6% ($p<0.05$), and 13.6% to 17.6% ($P<0.05$), respectively in Pt-S cells and from 12.8% to 18.7% ($p<0.05$), and 33.85% to 33% (n.s), respectively in Pt-R cells **(Fig. 3B)**. Treatment with HLM006474, an E2F1 inhibitor significantly reduced OA-induced cell proliferation in both Pt-S and Pt-R cells (**Fig. 3C**) validating observations from RNA-Seq and RPPA experiments. Based on these findings, we next examined whether E2F1 inhibition could also alter the response of OC cells to carboplatin. Pharmacological inhibition of E2F1 with HLM00474 (20 μM) resulted in significant reduced carboplatin IC_{50} values in both Pt-S (from 16.16 μM to 4.14 μM) and Pt-R (42.21 μM to 16.88 μM) OVCAR5 cells (**Fig. 3D**).

Analysis of the DEGs from the RNA-Seq data using EnrichR showed that OA induced the expression of minichromosome maintenance (MCM) genes (Supplementary **Figs. S2A-B**), which are essential for DNA replication, cell division and maintenance of genetic information [46]. The MCM complex is overexpressed in ovarian cancer [47], contributing to cell proliferation, genomic instability, and chemoresistance [48, 49]. Increased expression levels of MCM 2, MCM6, MCM7, and MCM10 in response to OA in Pt-S and Pt-R OVCAR5 cells were validated by quantitative RT-PCR (Supplementary **Figs. S2C-F)**. Analyses using Kaplan Meyer plots [50] and publicly available transcriptomic databases [51] show that high expression levels of MCM2, MCM6, MCM7 and

MCM10 are associated with decreased overall survival in OC patients (Supplementary **Figs. S2G-J**, $p<0.05$ for each of the transcripts). The settings and cutoffs for survival analyses included all OC subtypes, treatment groups, and GSE databases. Taken together, these results show that OA supports the proliferation of OC cells by promoting cell cycle progression, possibly via upregulation of MCM proteins and activation of E2F1 transcription regulator which support cancer cell growth under metabolic stress.

On the other hand, RNA-Seq analysis of OC cells treated with PA showed an increase in cellular stress and activation of pathways such as: *unfolded protein response, cellular response to stress, cellular response to stimuli, IRE1alpha, ATF6-alpha, and PERK* (Reactome 2022) as well as cell death pathways, such as *ferroptosis* (Wikipathway 2021 human; Supplementary **Fig. S3A**), perhaps explaining the observed decrease in cell viability after PA treatment. The main effectors of transcriptomic changes induced by PA were NFKB1, RELA, JUN, and ATF4 (Supplementary **Fig. S3B**).

Importantly, a significant increase in tumor volume ($P<0.05$) and numbers of peritoneal implants ($p<0.05$, **Figs. 3E-F)** were observed in mice implanted IP with Pt-R OVCAR5 cells and fed an OA enriched diet (10% OA content) vs. an isocaloric control diet (n=7 mice per group). There was no significant difference between body weights for mice maintained on the two diets (Supplementary Fig. **S4A-C**). To assess the effects of OA on cancer cell proliferation *in vivo*, harvested tumors were analyzed by IHC for Ki-67 expression. Ki67 proliferation index was upregulated in tumors collected from mice fed OA-enriched vs. control diet (**Figs. 3G-H**). Additionally, RNA-Seq analysis assessed transcriptomic changes induced by OA enriched diet in xenografts. There were 328 differentially expressed genes (FDR<0.05) and tumors from mice fed the OA diet harbored increased expression of cell cycle related pathways "*mitotic spindle", "G2M checkpoints", "E2F1 targets", "C-Myc targets"*

among others **(Figs. 3I-K)** consistent with observations from *in vitro* experiments. Together, these data support that OA promotes cell cycle progression, OC cell proliferation, and tumor growth *in vivo*.

Inhibiting lipid transport mediated by FABP4 re-sensitizes OC cells to platinum: Our previous work indicated that Pt-R cells uptake more FAs from the extracellular environment compared to Pt-S cells [52]. To identify the key players mediating lipid import and transport in OC cells, GFP transduced Pt-S or TomatoRed transduced Pt-R cells were directly co-cultured with mature VNPAD adipocytes for three days. The expression levels of fatty acid transporters and fatty acid binding proteins (FABPs) were measured via RT-qPCR before and after co-culture and separation via flow cytometry. Co-culture with adipocytes increased the expression levels of CD36 a key FA transporter and of FABP4, a lipid chaperone in Pt-R OC cells (**Fig. 4A**). The expression levels of the carrier proteins FABP4 and FABP5 were elevated at baseline in OVCAR5 Pt-R cells vs Pt-S cells, both at mRNA and protein level (**Fig. 4B**). Both FABP4 and FABP5 are known to transport long-chain fatty acids (LCFAs) such as OA, PA, stearic acid, and linoleic acid from receptors on the plasma membrane to cellular organelles [21]. Among the family of FABPs, FABP4 plays a key role in the cross talk between OC cells and adipocytes and is a key driver of peritoneal metastasis [53]. Based on these considerations and the observations that FABP4/5 were upregulated in resistant vs sensitive cells, we tested the effects of BMS-309403, an FABP4/5 inhibitor. The drug did not significantly inhibit cancer cell viability at doses less than 400nM (Supplementary **Fig. S5A**). At non-cytotoxic doses, the inhibitor reduced OA-induced rescue of cell proliferation under low serum conditions (**Fig. 4C**). Additionally, treatment with BMS-309403 reduced the expression levels of the transcription factor E2F1 and of other components of the Rb-E2F1 cell cycle pathway, such as phosphorylated RB (pRB) and Cyclin D1 found to be activated by OA supplementation (**Fig. 4D**). Effects of BMS-309403 on OA-induced E2F1 and cyclin D1 expression were more pronounced in Pt-R compared to Pt-S cells (**Fig. 4D**). Additionally, at non cytotoxic levels (350nM), BMS-309403 re-sensitized Pt-R OC cells to cisplatin *in vitro*. Treatment with the FABP

418 inhibitor reduced the Pt IC50 in Pt-R cells (from 11.893 μM to 5.0415 μM in OVCAR5 cells (**Fig. 4F**).
419 A similar trend with improved sensitivity to Pt was observed in PEO4 cells co-treated with BMS-
420 309403 **(**Supplementary **Fig. S5B**). The effects of the inhibitor on response to Pt were modest in Pt-S
421 OVCAR5 (**Fig. 4E**) and PEO1 cells (Supplementary **Fig. S5B**).

422 **FABP4 inhibition reduces OC progression in vivo:** We next tested the effects of the FABP inhibitor
423 in Pt-R OC xenografts and patient derived xenografts (PDX) in vivo. Female nude mice carrying
424 intraperitoneal (ip) Pt-R OVCAR5 xenografts were randomly assigned to ip treatment with BMS-
425 309403 (15 mg/kg) daily (5 times per week), carboplatin (20 mg/kg weekly), the combination, or
426 vehicle (control). The experimental design is included in Supplementary **Fig. S5C** (n=7 mice per
427 group). Carboplatin did not significantly alter the number of peritoneal nodules, the total tumor volume,
428 or tumor weight, as anticipated for xenografts derived from Pt-R OC cells (**Figs. 5A-C**). Mice treated
429 with BMS-309403 alone developed significantly lower numbers of peritoneal tumors and displayed a
430 trend towards decreased tumor weights and volumes compared to control mice (**Figs. 5A-C**). Mice that
431 received the combination treatment had significantly lower numbers of tumors and reduced tumor
432 weight ($p<0.05$) compared to the control and carboplatin-treated groups (**Figs. 5 A-C**). There was
433 modest decrease in body weight induced by BMS-309403 and by the combination treatment
434 (Supplementary **Fig. S6A**). To assess the effects of treatment on cancer cell proliferation, Ki-67
435 expression was assessed in xenografts and found to be significantly reduced in tumors collected from
436 mice treated with the FABP inhibitor and with the combination treatment (**Figs. 5D-E**), supporting that
437 blocking lipid uptake inhibits cell proliferation.

438 Treatment with BMS-309403 was also tested in a subcutaneous (sq) Pt-R ovarian PDX previously
439 described [29]. Treatment with the FABP4 inhibitor over 5 weeks decreased average tumor weights
440 (**Fig. 5F**) and volumes (**Figs. 5G-H**) compared to vehicle. The mixed effects model showed that tumor

441 growth was significantly faster in the control vs. BMS309403 treated mice (interaction p = 0.014).
442 Differences began to emerge around Day 21 (p=0.053), persisting at Day 28 (p=0.015) and Day 35 (p
443 = 0.007). Treatment with BMS-309403 induced mild decrease in mouse body weights (Supplementary
444 **Figs. S6 B-C**).

445 To determine the effects of treatment on lipid content in tumors, we used stimulated Raman
446 spectroscopy (SRS) on tissue slides from xenografts treated with control, BMS-309403, carboplatin or
447 the combination. After deconvoluting cellular and matrix components, SRS imaging indicated a trend
448 towards diminished lipid versus protein content in the mapped cellular area of tumors in the group
449 treated with carboplatin and BMS-309403 vs. control, even though this difference did not reach
450 statistical significance (Supplementary **Figs. S7A-B**). Together, the data support that inhibiting lipid
451 transport mediated by FABP4 reduced the growth of Pt-R xenografts and PDXs *in vivo* by decreasing
452 tumor cell proliferation and reducing tumor lipid content.

453 **FABP4 is highly expressed in metastatic and recurrent tumors and FABP4 expression levels are**
454 **correlated with decreased survival**: Based on our findings showing that inhibiting FABP4
455 resensitizes the Pt-R cells to platinum *in vitro* and decreases tumor growth *in vivo* and the previous
456 reports linking FABP4 to OC metastasis [23], we assessed the expression of this lipid transporter in a
457 panel of 21 paired human ovarian tumors specimens, collected from primary, metastatic, and recurrent
458 tumors (**Fig. 6A**). IHC staining revealed that FABP4 expression quantified by an H score was
459 significantly upregulated in metastatic and recurrent lesions compared to primary tumors (**Fig. 6B**). To
460 further evaluate the significance of FABP4 to clinical outcomes, we used the Kaplan-Meier plotter in
461 publicly available clinically annotated OC genomic databases [50]. We included serous OC tumors and
462 all treatment groups. High FABP4 expression levels were associated with both decreased overall

survival and decreased progression free survival (**Fig. 6C**). These results highlight FABP4 as a potential prognostic biomarker and therapeutic target in OC.

Discussion

Here we show how exogenous lipids affect the proliferation and tumorigenicity of OC cells and report that Pt-R OC cells are highly dependent on OA for growth. Compared to previous findings from our and other groups [3, 25, 29, 54], these results show differences in how saturated and unsaturated FAs modulate cell behavior in nutrient-deprived conditions, with OA playing a key role in maintaining cell proliferation and stimulating tumor growth. The novelty of this study comes from showing the platinum resistant cells' dependence on unsaturated FAs and the impact of dietary OA on ovarian tumor growth. We applied SRS microscopy to measure lipid content in tumors, demonstrating feasibility of the approach in whole tissue. Ultimately our findings identify potential new therapeutic interventions targeting lipid transport to inhibit the growth of resistant tumors and highlight the effects of diet on tumor growth. These results have several implications.

First, we show that OA was the primary FA responsible for rescuing the proliferation of Pt-R OC cells under nutrient-deprived conditions. This is consistent with previous reports showing that OA, a monounsaturated fatty acid, enhances cell survival and growth of cancer cells by influencing membrane dynamics and energy metabolism [17, 55, 56]. RNA sequencing and proteomics analysis of OA treated cells show activation of cell proliferation pathways and identify the E2 promoter binding factor 1 *(E2F1)* as a key regulator of the transcriptomic changes induced by OA. Induction of E2F1 transcription by OA was previously observed in pre-adipocytes [57], but the mechanism by which this occurs remains not known. OA may affect transcription by directly binding the peroxisome proliferator-activated receptors (PPARα and δ), indirectly by activating the SREBP1 transcription factor, or by activating cell signaling at the plasma membrane [58]. Here we show that inhibition of

the carrier FABP4 protein attenuates OA-induced E2F1 activation, suggesting that inhibiting lipid transfer attenuates the activity of this pathway. E2F1 regulates expression of genes involved in cell cycle progression and is essential for oncogenesis [59].

Importantly we also show that an OA enriched diet promoted tumor growth in an IP OC model, suggesting that dietary fat can stimulate peritoneal dissemination of Pt-R ovarian xenografts, and further emphasizing the impact that exogenous lipids can have to tumor progression. The observations that OA promote cancer cell fitness under conditions of nutritional stress, as those observed in the tumor microenvironment of rapidly growing tumors, are consistent with previous reports documenting the pro-oncogenic functions of the FA desaturase SCD1, which catalyzes the conversion of stearic acid into OA. We had previously reported increased SCD1 expression in ovarian tumors and showed that the enzyme regulates the survival of cancer cells by maintaining the balance between UFAs and SFAs [17]. SCD1 overexpression led to increased UFA levels and conferred bioenergetic advantage in other cancers, such as colon, triple negative breast, and prostate cancer [60] while SCD inhibitors exerted anti-tumor effects [18, 19], further underscoring the effects of the enzyme's end-product, OA, on cancer cells.

In contrast, PA, a saturated FA, induced cellular stress as evidenced by activation of JUN and ATF4, and reduced cell proliferation. Initial activation of ATF4 plays a protective role, however prolonged upregulation leads to induction of CHOP and apoptosis [61]. Likewise, JUN activation plays either a pro-survival or pro-apoptotic role. Under conditions of stress, JUN/AP1 activation drives transcription of pro-apoptotic genes, leading to cell death [62]. The findings are supported by the existing literature suggesting that PA, by promoting oxidative stress and inflammation, leads to cellular dysfunction and apoptosis [63]. Thus, while OA seems to protect Pt-R OC cells from the adverse effects of nutrient deprivation, PA increases the stress response. These results are consistent with a recent report

demonstrating that a SFAs rich diet depleted of oleic acid inhibits tumor growth by upregulating stress pathways in cancer cells [64]. In sum, our findings show the distinct roles that different FA classes play in regulating cancer cell behavior, which could have important implications for understanding tumor metabolism and guide potential dietary interventions to affect tumor growth and response to therapy [65]. Interestingly, a direct correlation between dietary fat, including both saturated and unsaturated fatty acids, and clinical outcomes of OC was recently reported in a prospective cohort analysis, underscoring the clinical significance of lipid intake to tumor progression [64].

Lastly, we show that the effects of OA on Pt-R cells involve the fatty acid-binding proteins (FABPs), carrier proteins which mediate import of FAs from the plasma membrane to mitochondria, endoplasmic reticulum and lipid droplets [21]. We noted increased FABP4 expression in metastatic versus primary ovarian tumors, consistent with previous observations [53]. Interestingly, here we also show that FABP4 expression is upregulated in recurrent versus primary tumors. Further, inhibition of FABP4 reversed the proliferative effects of OA under nutrient-deprived conditions. These findings highlight the importance of lipid transport regulating cancer cell metabolism and growth, suggesting that FABPs, and specifically FABP4, may be critical in driving the lipid-dependent phenotype observed in Pt-R OC cells [52]. We also demonstrated that the FABP4 inhibitor BMS-309403 re-sensitized Pt-R OC cells to platinum, both *in vitro* and *in vivo*. The effects of the inhibitor on resistant cells may be related to the higher dependence of Pt-R OC cells on fatty acid import [3]. BMS-309403 alone also inhibited the growth of a Pt-R PDX model. Interestingly, the antitumor effects of BMS-309403 were more evident *in vivo* than what was observed in cancer cells, suggesting that inhibition of lipid transport might exert indirect effects by altering non-cancer cells in the tumor microenvironment. These observations

suggest that targeting lipid uptake may represent an effective strategy to overcome chemoresistance in OC.

Remaining to be elucidated is the mechanism by which OA promotes cancer cell proliferation under conditions of nutritional stress. Our previous findings suggested that Pt-R cells preferentially use FAs for β-oxidation and energy generation and are highly susceptible to inhibition of this pathway by etomoxir [3]. However, it is possible that Pt-R cancer cells depend on FAs through other mechanisms linked to cell survival under stress. Additional studies are needed to validate FABP4 inhibition as a potential therapeutic intervention in cancer and to explore the broader implications of altering lipid metabolism either through inhibitors or through dietary modifications. It is important to note that such inhibitors also affect normal tissues, including immune cells, and their impact is expected to be more complex. In all, our results point to a novel vulnerability of chemo-resistant cancer cells and tumors which can be further explored as a cancer target.

Conclusions

The results reported in this article provide insight into a novel vulnerability of chemo-resistant OC tumors and show that platinum resistant cancer cells are highly dependent on unsaturated FAs for proliferation *in vitro* and *in vivo*. Inhibiting intracellular FA transport reduces Pt-R OC progression *in vivo*.

Data availability statement:

All data can be made available upon request. RNA-seq analysis results are deposited in GEO (GSE295220; token: yrafksyadzad)

Abbreviations

OC: Ovarian Cancer

HGSOC: High-Grade Serous Ovarian Cancer

Pt-S: Platinum sensitive

Pt-R: Platinum resistant

FA: Fatty Acids

SFA: Saturated Fatty Acids

MUFA: Mono-Unsaturated Fatty Acids

OA: Oleic Acid

PA: Palmitic Acid

FABP4: Fatty Acid Binding Protein 4

FABP5: Fatty Acid Binding Protein 5

CD36: Fatty acid translocase (FAT)

MCM2: DNA replication licensing factor MCM2

MCM6: DNA replication licensing factor MCM6

MCM7: DNA replication licensing factor MCM7

MCM10: DNA replication licensing factor MCM10

E2F1: Transcription factor E2F1

Acknowledgements

Tumor specimens were procured through the Pathology Core and sequencing was performed in the NUSeq Core supported by NCI CCSG P30 CA060553 awarded to the Robert H Lurie Comprehensive Cancer Center. Flow cytometry analyses were performed in the Northwestern University - Flow Cytometry Core Facility and histology services were provided by the Northwestern University Pathology Core supported by Cancer Center Support Grant NCI CA060553. We received support for

data analysis from the Quantitative Data Science Core supported by Cancer Center Support Grant NCI CA060553. Proliferation assays were performed in the Analytical bioNanoTechnology Equipment Core Facility of the Center for Regenerative Nanomedicine at Northwestern University. ANTEC receives partial support from the Soft and Hybrid Nanotechnology Experimental (SHyNE) Resource (NSF ECCS-2025633) and Feinberg School of Medicine, Northwestern University. This research was supported in part through the computational resources and staff contributions provided for the Quest high performance computing facility at Northwestern University which is jointly supported by the Office of the Provost, the Office for Research, and Northwestern University Information Technology. The Functional Proteomics RPPA Core receives partial support from the National Cancer Institute under grant P30CA016672 to MD Anderson Cancer Center.

Funding:

This research was supported by funding from the US Department of Veterans Affairs (BX006012 and BX006020) and the Diana Princess of Wales endowed Professorship from the Lurie Cancer Center to DM.

Author information

Department of Obstetrics and Gynecology, Feinberg School of Medicine, Northwestern University, Chicago, IL 60611, USA

Ana Maria Isac, Andres Valdivia, Yinu Wang, Didi Zha, Wenan Qiang, Vanessa Hernandez, Guangyuan Zhao, Annapurna Sai Josula, Ujin Kim & Daniela Matei

Department of Biomedical Engineering, Boston University, Boston, MA, 02155, USA

Chinmayee Vallabh Prabhu Dessai & Ji-Xin Cheng

David Geffen School of Medicine, University of California, Los Angeles (UCLA)

Sandra Orsulic

VA Greater Los Angeles Healthcare System, Los Angeles, CA, USA

Sandra Orsulic

Robert H. Lurie Comprehensive Cancer Center, Feinberg School of Medicine, Northwestern University, Chicago, IL 60611, USA

Daniela Matei

Jesse Brown VA Medical Center, Chicago, IL, 60612, USA

Daniela Matei

Contributions:

AMI designed, acquired, analysed and interpreted all *in vitro* data and wrote the manuscript. AFV assisted with experiment design, data acquisition and analysis. YW, WQ, VH and UK performed the animal experiments. GYZ and DZ analysed RNA- sequencing data. CPV analyzed lipid mapping experiments. SO acquired, annotated and provided the paired human tumor specimens used in this study. DM and JXQ designed the study, provided funding for the study, critically reviewed, edited and approved the manuscript.

Corresponding author

Daniela Matei, MD

Ethics declaration

Animal studies were approved by the Institutional Animal Care and Use Committee (IACUC) of Northwestern University (protocol IS00017063). Analyses using deidentified human tissue were approved by institutional IRB.

Consent for publication

Not applicable

Competing interests

The authors declare no conflict of interest related to this material.

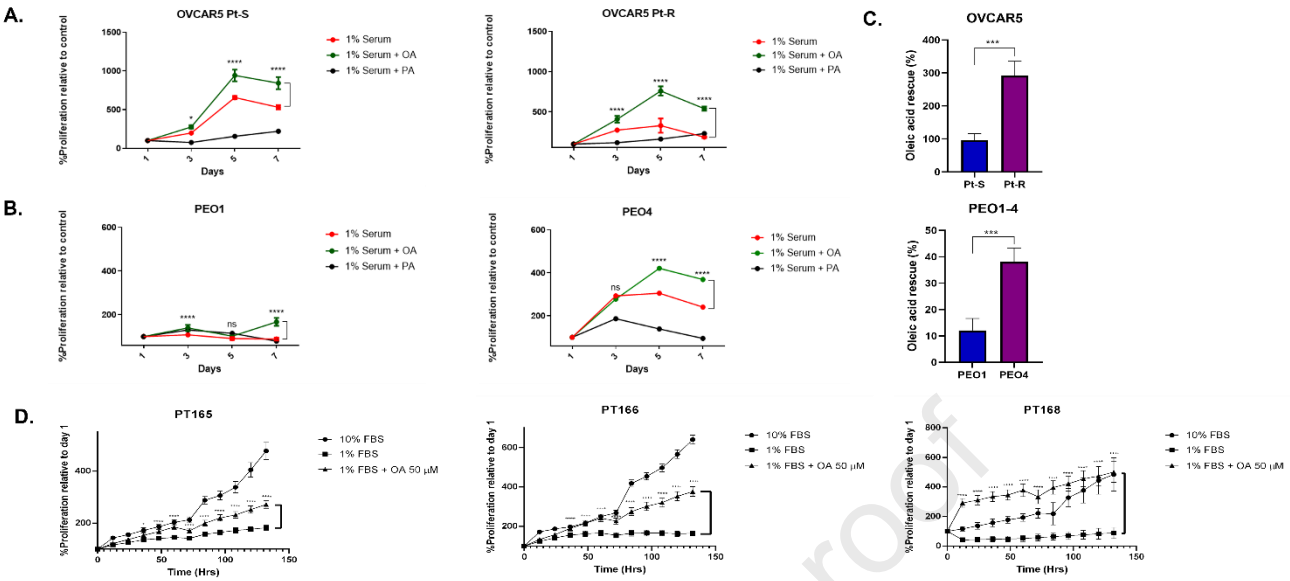

Figure 1. Oleic acid rescues viability of Pt-R vs Pt-S OC cells grown under serum restriction conditions. A-B Cell viability of Pt-R and Pt-S OVCAR5 (A) or PEO1 and PEO4 (B) cells was assessed by using the CCK-8 assay under several conditions: 1% serum, 1% serum supplemented with 50µM OA, and 1% serum supplemented with 50 µM PA. Cell viability was measured on days 1, 3, 5 and 7. **C.** The OA induced rescue (%) was calculated for Pt-S and Pt-R cells at day 7 as the relative increase in cell viability in the treatment group (OA) compared to control (1% serum), defined as: (mean treatment − mean control) / mean control × 100. **D.** Primary OC cells were cultured under low serum conditions and treated with 50 µM OA. Proliferation was monitored every 12 h during a 6-day period using the Incucyte® S3 Live-Cell Analysis System. Graphs present averages of three replicates at each time point relative to baseline. Two-way ANOVA statistical tests, with Tukey post-test were performed using the GraphPad Prism 7 software. n=3; *p<0.05, **p<0.005, ***p<0.0005.

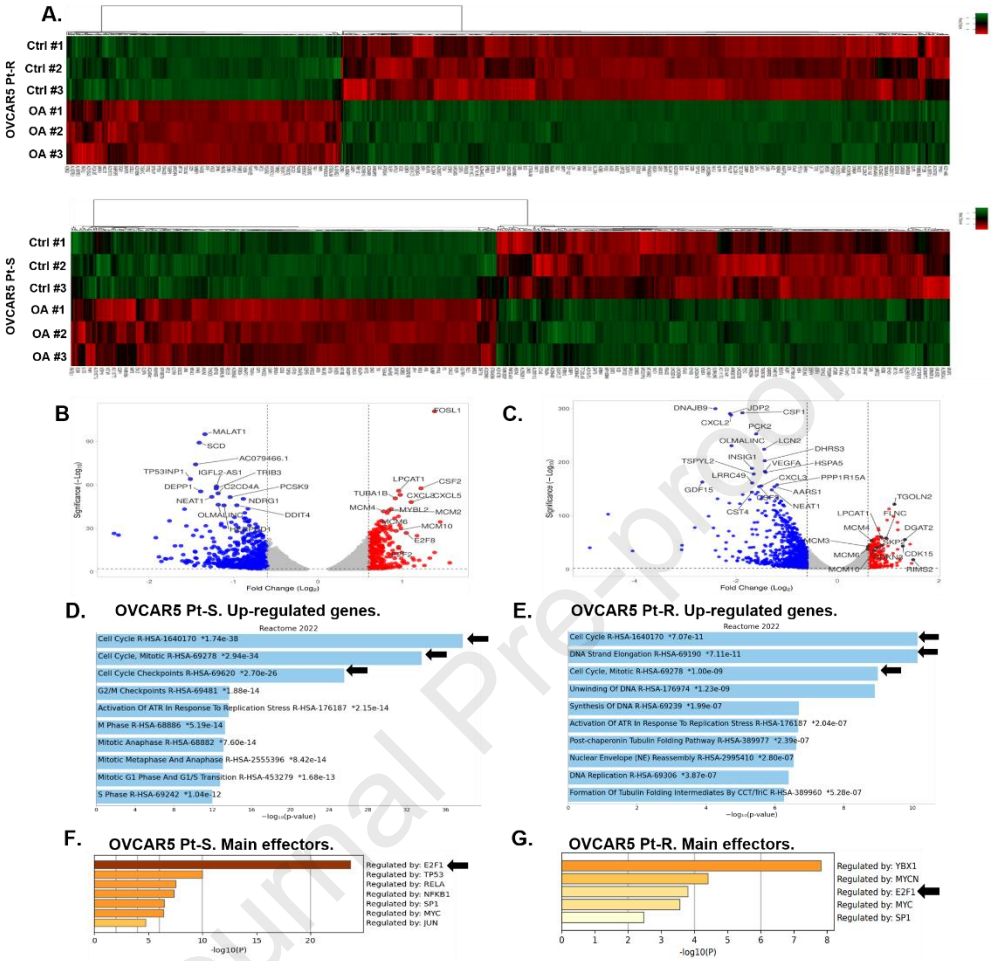

Figure 2. RNA-Seq analysis of Pt-S and Pt-R OVCAR5 cells treated with OA. A. Hierarchical clustering of the upregulated and downregulated DEGs in Pt-R (n= 1366 DEGs, FDR< 0.05) and Pt-S (n=973 DEGs, FDR <0.05) cells treated with OA (50μM) vs control (1% FBS); n=3 replicates per condition. **B-C.** Volcano plots show the top upregulated and downregulated genes in Pt-S **(B)** and Pt-R OVCAR5 cells treated with OA (50μM) vs control (1% FBS) **(C). D-E.** Pathway analysis of DEGs identified by RNA-Seq in Pt-S **(D)** and Pt-R **(E)** cells treated with OA (50μM) vs control (1% FBS). Pathway analysis of upregulated genes (fold change > 1.5, and FDR < 0.05) was performed by using EnrichR. **F-G** Metascape analysis of upregulated genes in Pt-R OVCAR5 cells treated with OA vs control (fold change > 1.5, FDR< 0.05) identified E2F1 as the main effector.

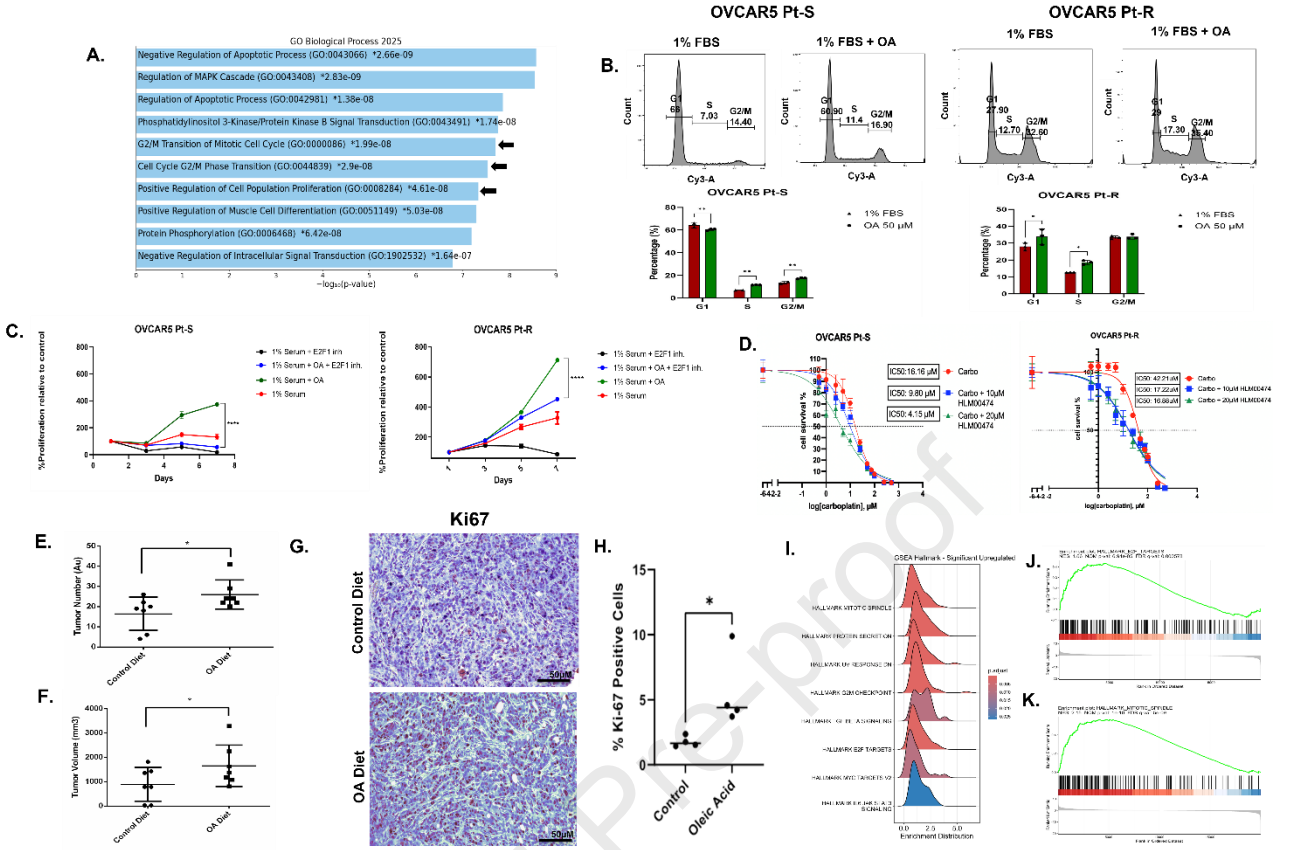

Figure 3. OA supports OC cell proliferation and tumor growth by promoting cell cycle progression. A. Pathway analysis in GO Biological process of significantly upregulated proteins (FDR <0.05) identified by RPPA in Pt-R cells treated with OA (50 µM) vs control (1% FBS); n=3 replicates per condition. Black arrows indicate cell cycle related pathways. **B.** Cell cycle analysis of Pt-S and Pt-R OVCAR5 cells and the quantification of the cells in various cycle phases. Cells were cultured under 1% FBS in the presence or absence of OA (50µM), stained with propidium iodine and analyzed via flow cytometry, graphs represent mean +/- SD percentage cells in G1, S and G2/M phase of 3 independent experiments; *p<0.05, **p<0.005 by two tailed t-test. **C.** E2F1 inhibition reverts OA induced cell proliferation. CCK8 assay measures cell proliferation of Pt-S and Pt-R OVCAR5 cells treated with OA (50µM) with and without the E2F1 inhibitor HLM00474 (20 µM). n=3 replicates. **D. Inhibition of E2F1 sensitizes OVCAR5 cells to carboplatin.** IC50 to carboplatin was measured in Pt-S and Pt-R OVCAR5 cells in the presence and absence of E2F1 inhibitor HLM00474 at

675 concentrations of 10 µM and 20 µM. Cell viability was measured after 72 h via CCK-8 assay. **E-F.**
676 Quantification of tumor numbers **(E)** and tumor volumes **(F)** of mice bearing ip Pt-R xenografts fed
677 with enriched OA diet v/s isocaloric diet, n=7 mice per group. **G-H**. Representative IHC images (40x)
678 (G) and quantification **(H)** showing Ki-67 positive cells in xenografts from mice fed control and OA
679 diet (n=4 per group). **I-K.** Pathway analysis of upregulated DEGs (fold change > 1.5, and FDR < 0.05)
680 identified by RNA-Seq analysis of xenograft tumors isolated from OA vs control diet groups shows
681 enrichment in cell cycle-related pathways **(I)**. GSEA conducted using Hallmark gene sets from Human
682 Molecular Signatures Database (MSigDB) identified "*E2F targets*" **(J)** and "*mitotic spindle genes*"
683 **(K)** as being enriched in tumors from OA diet fed mice. Results represent the means of 3 replicates
684 unless stated otherwise, *p<0.05, **p<0.005, ***p<0.0005 by two-way ANOVA and Tukey post-test.
685
686

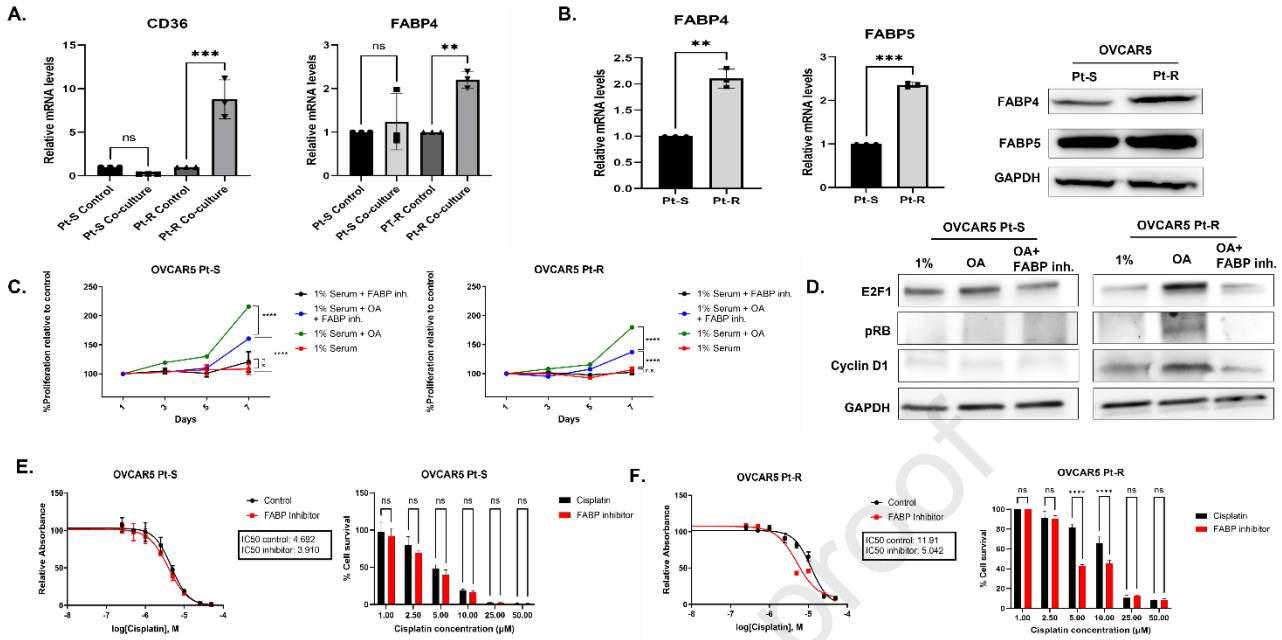

Figure 4. Inhibiting lipid transport mediated by FABP4 reverses OA induced rescue of cell viability and resensitizes Pt-R OC cells to platinum. A. Pt-S and Pt-R OVCAR5 cells were co-cultured with mature VNPAD adipocytes for three days and separated by FACS, mRNA expression levels of the CD36 transporter and FABP4 were measured by using RT-qPCR. n=3, ***p<0.0005 by one-way ANOVA follow by Tukey post-test **B.** Basal FABP4 and FABP5 mRNA and protein expression levels were measured in Pt-S and Pt-R OVACR5 cells by using RT-qPCR and western blotting, respectively. n=3, **p<0.005, ***p<0.0005 by two tailed t-test. **C..** BMS-309403 reduced OA-induced rescue of OC cell proliferation. Pt-S and Pt-R OVCAR5 cells were cultured under 1% FBS in the presence or absence of OA (50 μM) and the FABP inhibitor (350 nM). Cell proliferation was measured on days 1, 3, 5, and 7 by using the CCK8 assay, ****p<0.0001 by two-way ANOVA with Tukey post-test. **D.** Inhibition of FABPs reduced expression of E2F1 and components of the RB–E2F cell-cycle pathway. Pt-S and Pt-R OVCAR5 cells were cultured in 1% FBS for 24 h and then treated with 50 μM OA, with and without BMS-309403 200 nM, for an additional 24 h. Expression levels of E2F1, phosphorylated RB (pRB), and Cyclin D1 were measured using western blotting. N=3 replicates. **E-F.** Inhibition of FABPs re-sensitizes Pt-R OC cells to cisplatin. IC50 to cisplatin was

measured in Pt-S and Pt-R OVCAR5 cells in the presence and absence of BMS309403 at 350 nM concentration. Cell viability was measured after 72 h via CCK-8 assay.

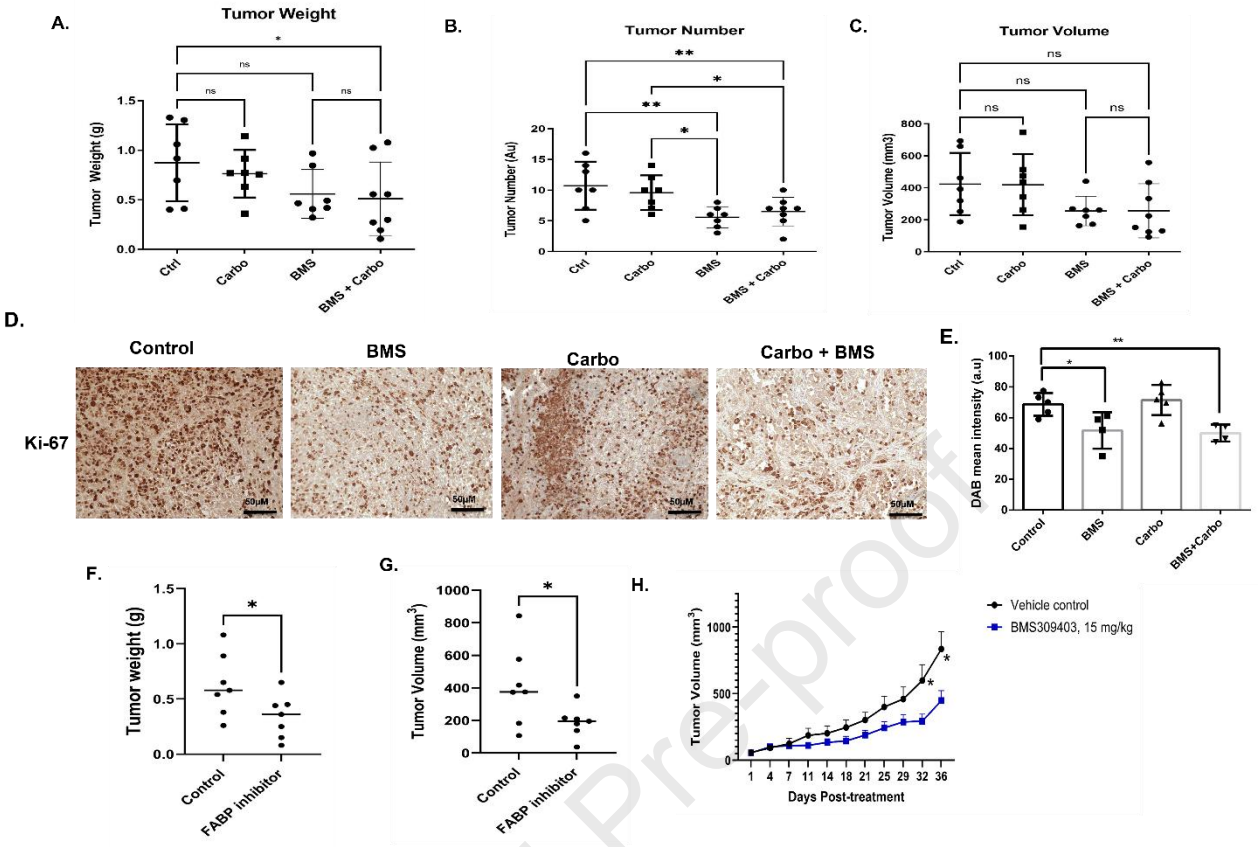

Figure 5. Inhibiting lipid transport mediated by FABP4 reduces OC xenograft growth in vivo. **A-C.** Mice bearing ip Pt-R xenografts were treated ip with vehicle, BMS-309403 (15 mg/kg daily), carboplatin (20 mg/kg weekly) or the combination for 28 days. Xenograft growth was assessed by determining **(A)** tumor weight, **(B)** number of peritoneal implants, and **(C)** tumor volume**;** n=7 mice per group. **D–E.** Representative IHC images **(D, 40**X magnification**)** and quantification **(E)** show the expression of the proliferation marker Ki-67 in xenografts collected from each group. Ki-67 expression was quantified by using the DAB deconvolution method and ImageJ software; n=5 xenografts per group. **F-H.** Ovarian cancer PDX tumor-bearing mice were treated IP daily with either vehicle control or 15 mg/kg BMS-309403. Differences in average tumor weights (F) and tumor volumes (G-H) are shown. Statistically significant differences are indicated (Day 32, p = 0.0452 and Day 36, p = 0.0291). *p<0.05, **p<0.005, ***p<0.0005 by one-way ANOVA with Tukey post-test and student t-test.

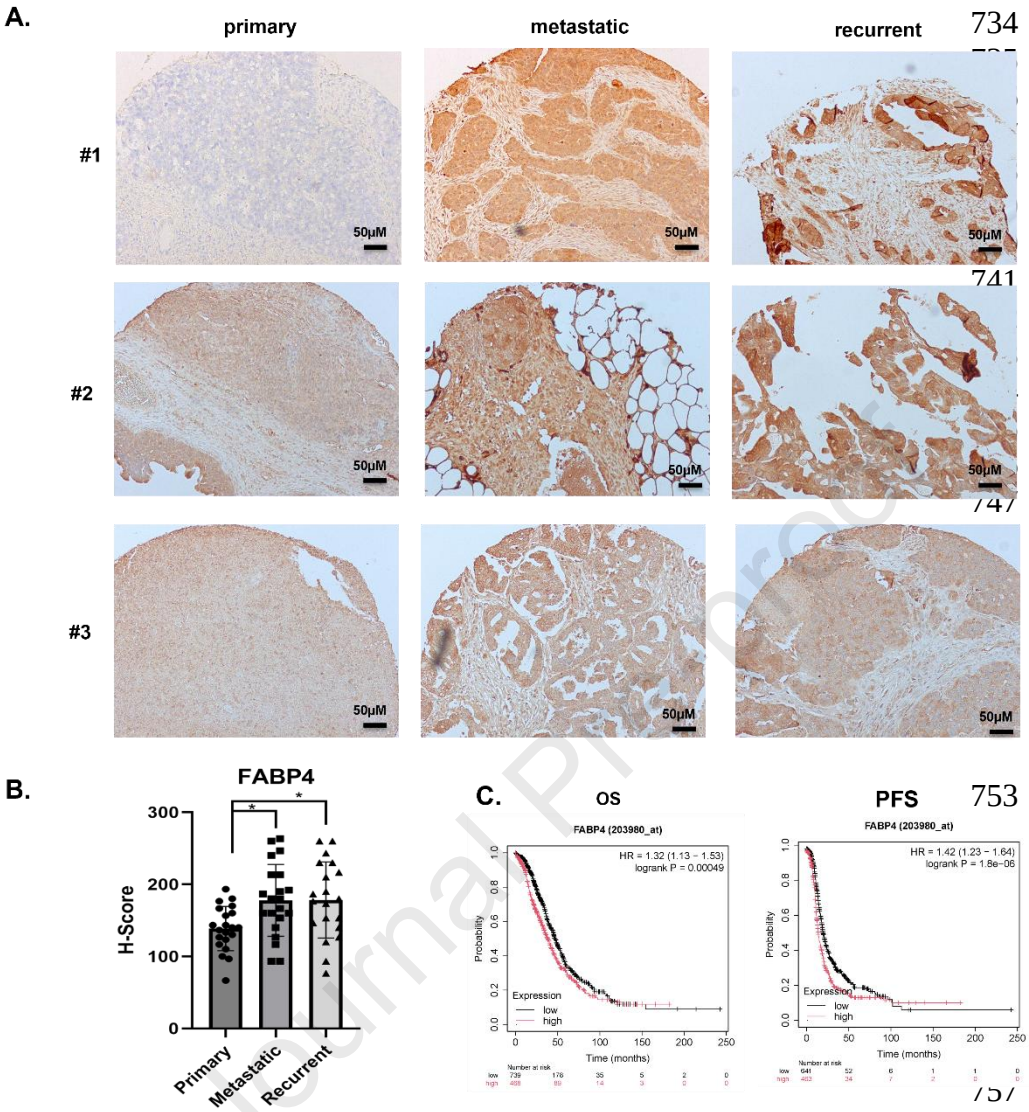

Figure 6. FABP4 expression in metastatic and recurrent HGSOC. A. Representative IHC images (20X magnification) show the expression of FABP4 in paired primary, metastatic and recurrent HGSOC tumors. **B.** Quantification of FABP4 staining performed by integrating staining intensity and percentage of positive cells, as an H score (n=21 paired HGSOC tumors, each tumor arrayed in triplicate. H score was calculated as staining intensity in cancer cells X percentage of cancer cells staining). **C.** Kaplan Meyer plot displays the correlation between FABP4 expression level (high vs. low) and overall survival (OS) or progression free survival (PFS) in serous OC tumors profiled in the GSE14764, GSE15622, GSE18520, GSE19829, GSE 23554, GSE26193, GSE26712, GSE27651,

766 GSE30161, GSE3149, GSE51373, GSE63885, GSE65986, GSE9891, and TCGA databases linked to
767 Kaplan Meier plotter.
768
769

REFERENCES

1. Veneziani, A.C., et al., *Heterogeneity and treatment landscape of ovarian carcinoma*. Nature Reviews Clinical Oncology, 2023. **20**(12): p. 820-842.
2. Wang, Y., et al., *Biology-driven therapy advances in high-grade serous ovarian cancer*. J Clin Invest, 2024. **134**(1).
3. Tan, Y., et al., *Metabolic reprogramming from glycolysis to fatty acid uptake and beta-oxidation in platinum-resistant cancer cells*. Nat Commun, 2022. **13**(1): p. 4554.
4. Hwang, S.-H., et al., *Oleic acid from cancer-associated fibroblast promotes cancer cell stemness by stearoyl-CoA desaturase under glucose-deficient condition*. Cancer Cell International, 2022. **22**(1): p. 404.
5. Marcial-Medina, C., et al., *Oleic acid induces migration through a FFAR1/4, EGFR and AKT-dependent pathway in breast cancer cells*. Endocr Connect, 2019. **8**(3): p. 252-265.
6. Giulitti, F., et al., *Anti-tumor Effect of Oleic Acid in Hepatocellular Carcinoma Cell Lines via Autophagy Reduction*. Frontiers in Cell and Developmental Biology, 2021. **9**.
7. Kim, H.S., et al., *Different Biological Action of Oleic Acid in ALDHhigh and ALDHlow Subpopulations Separated from Ductal Carcinoma In Situ of Breast Cancer*. PLOS ONE, 2016. **11**(9): p. e0160835.
8. Sales-Campos, H., et al., *An overview of the modulatory effects of oleic acid in health and disease*. Mini reviews in medicinal chemistry, 2013. **13**(2): p. 201-210.
9. Schwingshackl, L. and G. Hoffmann, *Monounsaturated fatty acids and risk of cardiovascular disease: synopsis of the evidence available from systematic reviews and meta-analyses*. Nutrients, 2012. **4**(12): p. 1989-2007.
10. Piccinin, E., et al., *Role of Oleic Acid in the Gut-Liver Axis: From Diet to the Regulation of Its Synthesis via Stearoyl-CoA Desaturase 1 (SCD1)*. Nutrients, 2019. **11**(10).
11. Martínez, M. and I. Mougan, *Fatty acid composition of human brain phospholipids during normal development*. Journal of neurochemistry, 1998. **71**(6): p. 2528-2533.
12. Reilly, N.A., et al., *Oleic acid triggers metabolic rewiring of T cells poising them for T helper 9 differentiation*. iScience, 2024. **27**(4).
13. Chen, J., et al., *Oleic acid decreases the expression of a cholesterol transport-related protein (NPC1L1) by the induction of endoplasmic reticulum stress in CaCo-2 cells*. Journal of physiology and biochemistry, 2011. **67**: p. 153-163.
14. Yang, Z.-H., et al., *Differential effect of dietary supplementation with a soybean oil enriched in oleic acid versus linoleic acid on plasma lipids and atherosclerosis in LDLR-deficient mice*. International Journal of Molecular Sciences, 2022. **23**(15): p. 8385.
15. Bhattacharjee, B., et al., *Oleic acid protects against cadmium induced cardiac and hepatic tissue injury in male Wistar rats: A mechanistic study*. Life sciences, 2020. **244**: p. 117324.
16. Santa-María, C., et al., *Update on Anti-Inflammatory Molecular Mechanisms Induced by Oleic Acid*. Nutrients, 2023. **15**(1): p. 224.
17. Zhao, G., et al., *Ovarian cancer cell fate regulation by the dynamics between saturated and unsaturated fatty acids*. Proceedings of the National Academy of Sciences, 2022. **119**(41): p. e2203480119.
18. Doria, M.L., et al., *Fatty acid and phospholipid biosynthetic pathways are regulated throughout mammary epithelial cell differentiation and correlate to breast cancer survival*. FASEB J, 2014. **28**(10): p. 4247-64.
19. Fritz, V., et al., *Abrogation of de novo lipogenesis by stearoyl-CoA desaturase 1 inhibition interferes with oncogenic signaling and blocks prostate cancer progression in mice*. Mol Cancer Ther, 2010. **9**(6): p. 1740-54.

20. Southam, A.D., et al., *Drug Redeployment to Kill Leukemia and Lymphoma Cells by Disrupting SCD1-Mediated Synthesis of Monounsaturated Fatty Acids.* Cancer Res, 2015. **75**(12): p. 2530-40.
21. Furuhashi, M. and G.S. Hotamisligil, *Fatty acid-binding proteins: role in metabolic diseases and potential as drug targets.* Nat Rev Drug Discov, 2008. **7**(6): p. 489-503.
22. Soto-Avellaneda, A. and B.E. Morrison, *Signaling and other functions of lipids in autophagy: a review.* Lipids in Health and Disease, 2020. **19**(1): p. 214.
23. Gharpure, K.M., et al., *FABP4 as a key determinant of metastatic potential of ovarian cancer.* Nature Communications, 2018. **9**(1): p. 2923.
24. Mukherjee, A., et al., *Adipocyte-Induced FABP4 Expression in Ovarian Cancer Cells Promotes Metastasis and Mediates Carboplatin Resistance.* Cancer Res, 2020. **80**(8): p. 1748-1761.
25. Wang, Y., et al., *Nanoparticle Targeting in Chemo-Resistant Ovarian Cancer Reveals Dual Axis of Therapeutic Vulnerability Involving Cholesterol Uptake and Cell Redox Balance.* Adv Sci (Weinh), 2024: p. e2305212.
26. Murphy, A.R., et al., *The Impact of High Adiposity on Endometrial Progesterone Response and Metallothionein Regulation.* J Clin Endocrinol Metab, 2024. **109**(11): p. 2920-2936.
27. Vu, B.G., et al., *Staphylococcal superantigens stimulate immortalized human adipocytes to produce chemokines.* PLoS One, 2013. **8**(10): p. e77988.
28. Gadupudi, G., et al., *PCB126 inhibits adipogenesis of human preadipocytes.* Toxicol In Vitro, 2015. **29**(1): p. 132-41.
29. Wang, Y., et al., *Frizzled-7 Identifies Platinum-Tolerant Ovarian Cancer Cells Susceptible to Ferroptosis.* Cancer Res, 2021. **81**(2): p. 384-399.
30. Valdivia, A., et al., *Complement activation at the interface between adipocytes and cancer cells drives tumor progression.* JCI Insight, 2025. **10**(6).
31. Huang, H., et al., *FTO-Dependent N (6)-Methyladenosine Modifications Inhibit Ovarian Cancer Stem Cell Self-Renewal by Blocking cAMP Signaling.* Cancer Res, 2020. **80**(16): p. 3200-3214.
32. Zhou, Y., et al., *Metascape provides a biologist-oriented resource for the analysis of systems-level datasets.* Nat Commun, 2019. **10**(1): p. 1523.
33. Chen, E.Y., et al., *Enrichr: interactive and collaborative HTML5 gene list enrichment analysis tool.* BMC Bioinformatics, 2013. **14**: p. 128.
34. Tan, Y., H. Lin, and J.X. Cheng, *Profiling single cancer cell metabolism via high-content SRS imaging with chemical sparsity.* Sci Adv, 2023. **9**(33): p. eadg6061.
35. Ni, H., et al., *High-content stimulated Raman histology of human breast cancer.* Theranostics, 2024. **14**(4): p. 1361-1370.
36. Liao, C.S., et al., *Denoising Stimulated Raman Spectroscopic Images by Total Variation Minimization.* J Phys Chem C Nanomater Interfaces, 2015. **119**(33): p. 19397-19403.
37. Ni, H., et al., *High-content stimulated Raman histology of human breast cancer.* Theranostics, 2024. **14**(4): p. 1361-1370.
38. Lior, C., et al., *Mapping the tumor stress network reveals dynamic shifts in the stromal oxidative stress response.* Cell Reports, 2024. **43**(5).
39. Zhao, G., H. Cardenas, and D. Matei, *Ovarian Cancer-Why Lipids Matter.* Cancers (Basel), 2019. **11**(12).
40. Langdon, S.P., et al., *Characterization and properties of nine human ovarian adenocarcinoma cell lines.* Cancer Res, 1988. **48**(21): p. 6166-72.
41. Musa, J., et al., *MYBL2 (B-Myb): a central regulator of cell proliferation, cell survival and differentiation involved in tumorigenesis.* Cell Death & Disease, 2017. **8**(6): p. e2895-e2895.
42. Morgunova, E., et al., *Structural insights into the DNA-binding specificity of E2F family transcription factors.* Nature Communications, 2015. **6**(1): p. 10050.

43. Deng, J., et al., *CXCL5: A coachman to drive cancer progression.* Front Oncol, 2022. **12**: p. 944494.
44. Wu, J., et al., *Skp2 modulates proliferation, senescence and tumorigenesis of glioma.* Cancer Cell International, 2020. **20**(1): p. 71.
45. Zhang, L.P., et al., *CDKN3 knockdown reduces cell proliferation, invasion and promotes apoptosis in human ovarian cancer.* Int J Clin Exp Pathol, 2015. **8**(5): p. 4535-44.
46. Neves, H. and H.F. Kwok, *In sickness and in health: The many roles of the minichromosome maintenance proteins.* Biochim Biophys Acta Rev Cancer, 2017. **1868**(1): p. 295-308.
47. Li, Y., et al., *Systemic Analysis of the DNA Replication Regulator MCM Complex in Ovarian Cancer and Its Prognostic Value.* Front Oncol, 2021. **11**: p. 681261.
48. Tian, Y., et al., *Research progress in MCM family: Focus on the tumor treatment resistance.* Biomedicine & Pharmacotherapy, 2024. **173**: p. 116408.
49. Wang, Y., et al., *MCM family in gastrointestinal cancer and other malignancies: From functional characterization to clinical implication.* Biochimica et Biophysica Acta (BBA) - Reviews on Cancer, 2020. **1874**(2): p. 188415.
50. Gyorffy, B., *Discovery and ranking of the most robust prognostic biomarkers in serous ovarian cancer.* Geroscience, 2023. **45**(3): p. 1889-1898.
51. Denkert, C., et al., *A prognostic gene expression index in ovarian cancer - validation across different independent data sets.* J Pathol, 2009. **218**(2): p. 273-80.
52. Tan, Y., et al., *Metabolic reprogramming from glycolysis to fatty acid uptake and beta-oxidation in platinum-resistant cancer cells.* Nature Communications, 2022. **13**(1): p. 4554.
53. Nieman, K.M., et al., *Adipocytes promote ovarian cancer metastasis and provide energy for rapid tumor growth.* Nat Med, 2011. **17**(11): p. 1498-503.
54. Avellino, A., et al., *An Olive Oil-Based High-Fat Diet Promotes Obesity-Driven Metastasis of Triple-Negative Breast Cancer.* Cancer Res, 2025.
55. Kado, T., et al., *Oleic acid stimulates cell proliferation and BRD4–L-MYC-dependent glucose transporter transcription through PPARα activation in ovarian cancer cells.* Biochemical and Biophysical Research Communications, 2023. **657**: p. 24-34.
56. Tamaki, T. and N. Fukushima, *Oleic acid stimulates proliferation of RMG-1 ovarian cancer cells by activating the pentose phosphate pathway and glutamine metabolism.* Biochem Biophys Res Commun, 2024. **722**: p. 150162.
57. Wang, Z., et al., *Dynamics of transcriptome changes during subcutaneous preadipocyte differentiation in ducks.* BMC Genomics, 2019. **20**(1): p. 688.
58. Santa-Maria, C., et al., *Update on Anti-Inflammatory Molecular Mechanisms Induced by Oleic Acid.* Nutrients, 2023. **15**(1).
59. Valdivia, A., et al., *E2F1 mediates competition, proliferation and response to cisplatin in cohabitating resistant and sensitive ovarian cancer cells.* Frontiers in Oncology, 2024. **14**.
60. Sanchez-Martinez, R., et al., *A link between lipid metabolism and epithelial-mesenchymal transition provides a target for colon cancer therapy.* Oncotarget, 2015. **6**(36): p. 38719-36.
61. Chai, H., et al., *Endoplasmic reticulum stress-mediated programmed cell death in the tumor microenvironment.* Cell Death Discov, 2025. **11**(1): p. 559.
62. Pinal, N., et al., *Short-term activation of the Jun N-terminal kinase pathway in apoptosis-deficient cells of Drosophila induces tumorigenesis.* Nat Commun, 2018. **9**(1): p. 1541.
63. Zhao, Z., et al., *Palmitic Acid Exerts Anti-Tumorigenic Activities by Modulating Cellular Stress and Lipid Droplet Formation in Endometrial Cancer.* Biomolecules, 2024. **14**(5).
64. AL Weir, S.L., M Li, CW Tan, S Ramus and NM Davidson, *IdentifiHR: predicting homologous recombination deficiency in high-grade serous ovarian carcinoma using gene expression.* BIORxiv.

913 65. Hoy, A.J., S.R. Nagarajan, and L.M. Butler, *Tumour fatty acid metabolism in the context of*
914 *therapy resistance and obesity*. Nature Reviews Cancer, 2021. **21**(12): p. 753-766.

915

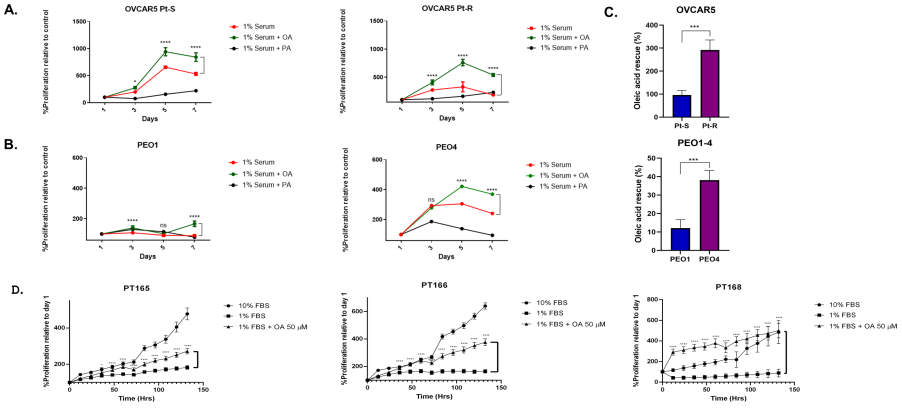

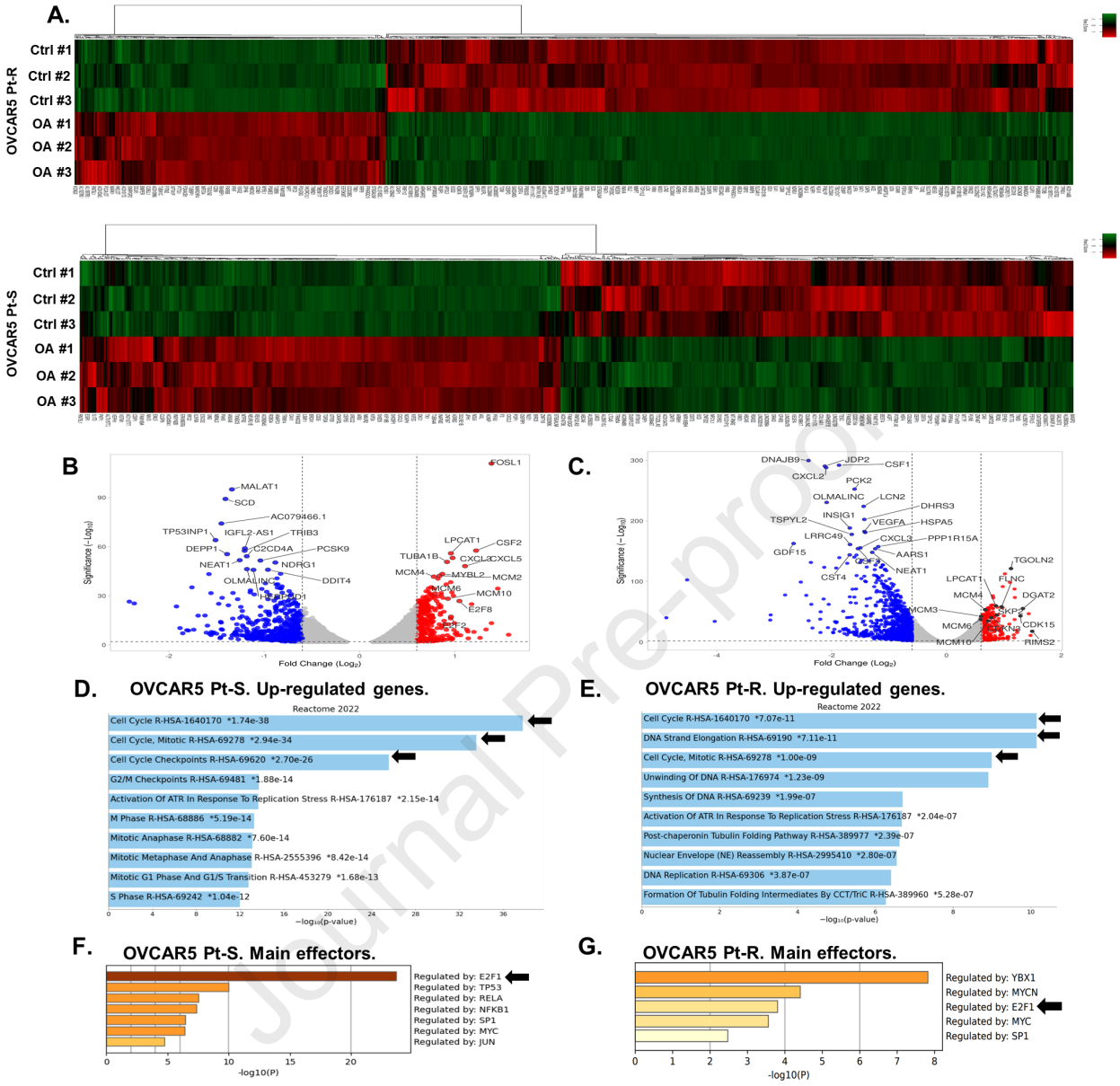

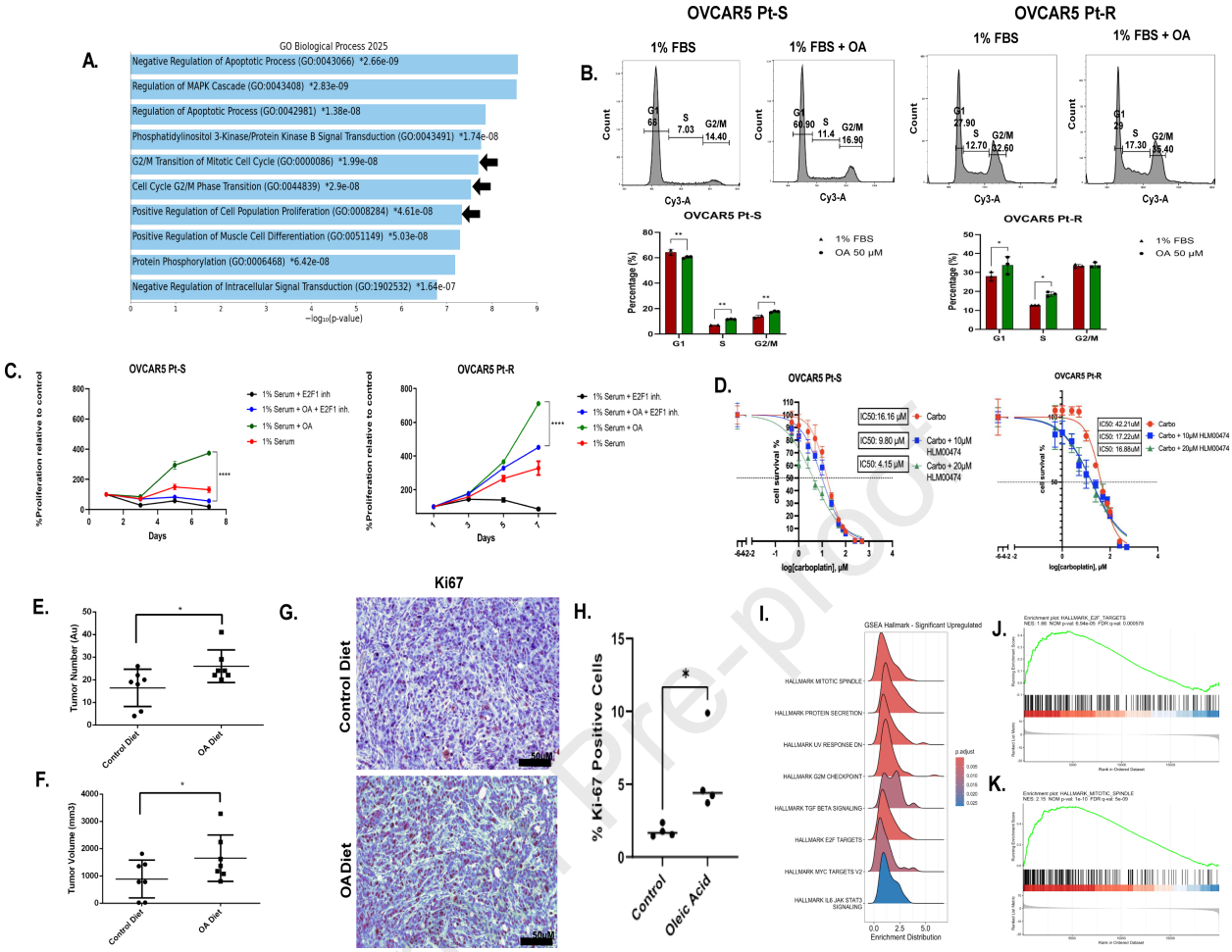

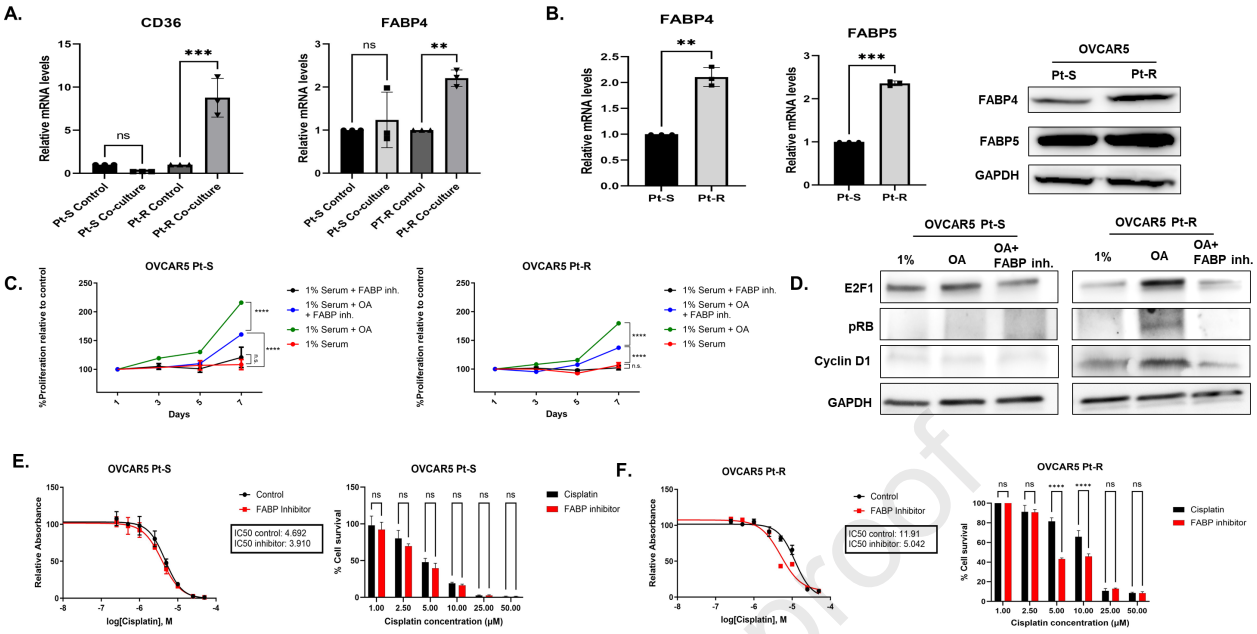

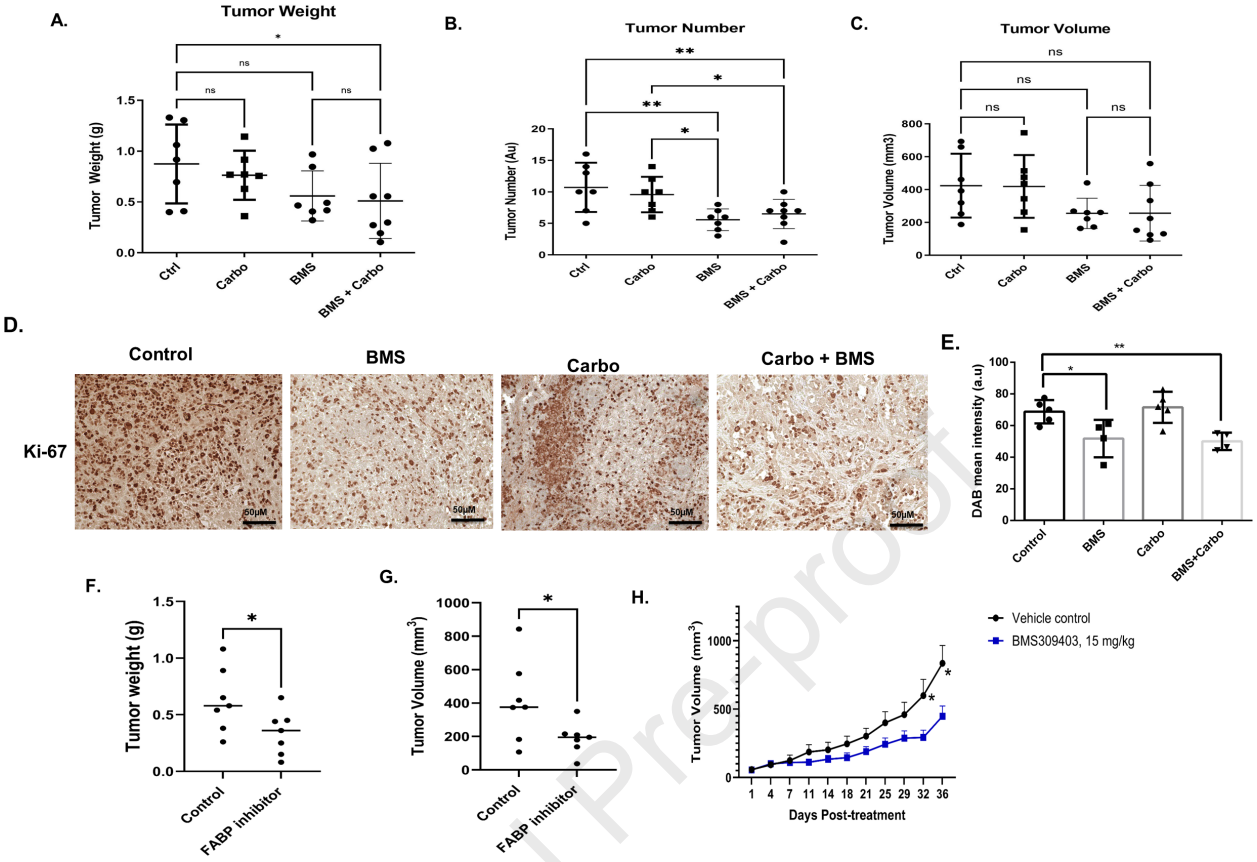

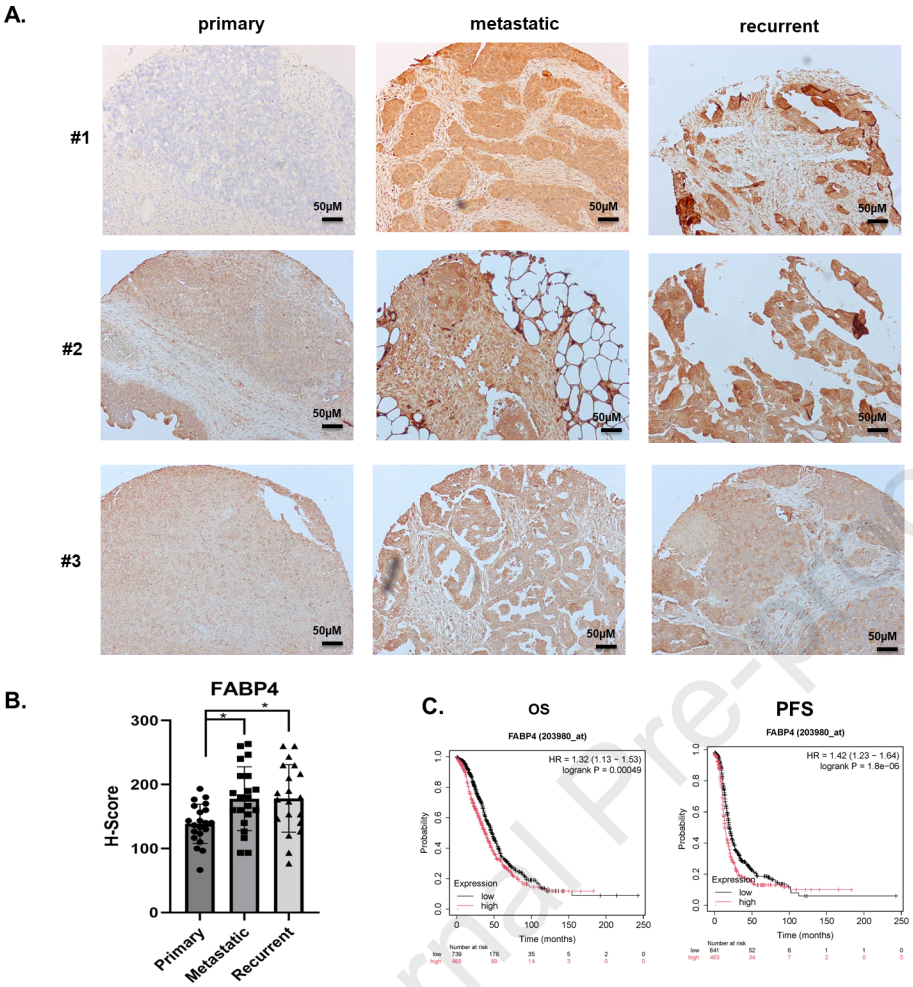

Title: Oleic Acid Fuels Cisplatin-Resistant Ovarian Cancer Through FABP4-Driven Lipid Uptake

Highlights:

- Proliferation of platinum resistant ovarian cancer cells is highly dependent on oleic acid which augmented proliferation and cell cycle related pathways leading to increased G2-M and S phase transition.
- A diet rich in oleic acid stimulated intraperitoneal platinum resistant ovarian xenograft growth and upregulated key pathways involved in cell cycle progression.
- Platinum resistant cancer cells and metastatic and recurrent ovarian tumors upregulate the lipid transporters FABP4 and CD36.
- Pharmacological inhibition of FABP4 reversed resistance to platinum and inhibited the growth of ovarian cancer xenografts and patient derived xenografts.
- Our findings point to the potential impact of dietary fat on tumor progression and resistance to treatment.

Title: Oleic Acid Fuels Cisplatin-Resistant Ovarian Cancer Through FABP4-Driven Lipid Uptake

Conflict of interest: The authors declare no conflict of interest related to this material.